Durham E-Theses

Equipment for the production and assessment of thin-film display devices

Martin, P. G.

How to cite:

Martin, P. G. (1970) *Equipment for the production and assessment of thin-film display devices*, Durham theses, Durham University. Available at Durham E-Theses Online: http://etheses.dur.ac.uk/10067/

Use policy

EQUIPMENT FOR THE PRODUCTION AND ASSESSMENT

OF THIN-FILM DISPLAY DEVICES

by

P. G. Martin B.Sc.

A thesis presented in canditature for the degree of Master

of Science in the University of Durham,   July 1970.

ABSTRACT

Work carried out in the Department on solid-state display devices based on thin films of willemite (Zn_2SiO_4:Mn) on silicon substrates has shown the need for a cleaner vacuum environment during preparation, and particularly has shown the usefulness of capacitance-voltage measurements in determining the physical behaviour of the structures. Other workers have shown the use of conductance-voltage measurements also. This thesis describes equipment designed and built to meet the above requirements.

A stainless steel ultra-high vacuum system, with an electron beam evaporator and provision for an electron bombard-ment substrate heater is described for use in the fabrication of thin film display devices. A clean environment at pressures down to 10^{-8} torr is provided by sorption and sputter ion pumps. The apparatus includes electronic equipment used for control n_o during long periods of unattended pumping, baking or evaporation.

Instrumentation for the assessment of the display devices (and other metal-insulator-semiconductor structures) has been developed, including a C-V Plotter, an I-V Plotter and a high performance conductance-capacitance (G-C-V) Plotter capable of

measuring device parameters over a wide range of values and
test frequencies.

ACKNOWLEDGEMENTS

CONTENTS

– Chapter 1 –

INTRODUCTION

1-1 Willemite display devices

Work carried out in the department by Edwards [1] has led to
the development of a solid-state display device consisting of
a thin film of willemite (Zn_2SiO_4:Mn) grown on a silicon
substrate. The luminescent films are formed by oxidising the
silicon surface, vacuum-evaporating electronic grade zinc
fluoride (activated by one per cent manganese fluoride), and
baking to $1100^{\circ}C$ to give the reaction:

$$ZnF_2\text{:Mn} + SiO_2 \rightarrow Zn_2SiO_4\text{:Mn} + SiF_4$$

When converted to willemite, these films gave bright green
cathodoluminescence, and weak electroluminescence.

Capacitance-voltage (C-V) measurements on the devices
showed that large numbers of impurity ions were present in the
insulating (willemite) layer, and it was decided to improve the
preparation environment by the use of an ultra-high vacuum
system and an electron beam evaporation source. It was also
suggested that a more detailed analysis of the physical behaviour
of the devices could be made by more thorough C-V measurements,

by conductance-voltage (G-V) measurements, and by current-voltage (I-V) measurements. It was hoped that these techniques might lead to more efficient electroluminescence, and to the production of useful display devices.

1-2 Equipment requirements

Previous vacuum evaporation of ZnF_2:Mn has been carried out in the pressure range 10^{-6} to 10^{-5} torr. Rotary and diffusion pumps had been used to achieve these pressures in a 12-inch bell jar system, in conjunction with a liquid nitrogen trap. It was considered that reducing the pressure to 10^{-8} or 10^{-9} torr would give some improvement in the cleanliness of the environment, and that the use of an electron beam evaporator would eliminate contamination by conventional resistively-heated crucibles. An ultra-high vacuum vessel, evacuated by sorption and sputter ion pumps, was designed and built, incorporating an electron beam evaporation source and provision for an electron bombardment substrate heater.

C-V measurements carried out on early devices used the prototype of the instrument described in Chapter 4. The instrument was inadequate in several respects, so a high performance conductance-capacitance (G-C-V) plotter was developed (Chapter 5). For examining contacts to devices, a versatile current-voltage (I-V) plotter was also designed and built (Chapter 6).

– Chapter 2 –

ULTRA-HIGH VACUUM SYSTEM

2-1 Clean vacuum equipment

The contamination problems associated with conventional rotary
pump/diffusion pump vacuum equipment are well understood, and the
presence of hydrocarbons and impurities from elastomer sealing
components is a hindrance in work with insulating thin films
on high purity silicon substrates. Although traps can be used
to improve the ultimate pressure attainable, newer types of
vacuum pump offer greater convenience and lower contamination
levels.

The uhv system designed and built for the willemite work
is based on sorption roughing pumps and a large sputter ion pump.
The ion pump is capable of pressures down to 10^{-7}-10^{-11} torr,
depending on outgassing and leak rates. Provision is also made
for adding a titanium sublimation pump for high pumping speeds
at low pressures. All three pumps are silent in operation, in
contrast to rotary pumps. Ion pumps are electronic, and pressures
between 10^{-4} and 10^{-8} torr can be measured directly from the
pump current.

The parts for the vacuum chamber were custom made from
stainless steel by Vacuum Generators Limited. Several ports are

provided for the connection of pumps, electrical connectors, an ion gauge, a window, and other accessories. The vessel was designed to hold an electron beam evaporator (Chapter 3) and an electron bombardment substrate heater.

Special stainless steels are available which make ideal vacuum fabrication material, and which are readily welded by a tungsten argon-shrouded arc. The stable welds made in this way have a low outgassing rate and do not seriously deteriorate with exposure to atmosphere. Clean electropolished stainless steel has an outgassing rate of less than 10^{-9} torr l s^{-1} cm^{-2}, or less than 10^{-12} torr l s^{-1} cm^{-2} after a vacuum bake. Vacuum stainless steels are stabilised by titanium or niobium against chromium carbide formation, which can create fine cracks in welded joints.

Ion pumps can be started at any pressure below 2.10^{-2} torr. Sorption pumps are used to rough down to about 10^{-2} torr, and have an ultimate pressure limited to 5.10^{-3} torr by neon and helium in the air. A sorption pump is a vessel containing a sorbent material (commonly Linde Molecular Sieve 5A) cooled by liquid nitrogen. The molecular sieve adsorbs atmospheric gases which are released when the pump returns to room temperature. The pump can be fully regenerated by heating to $300^{\circ}C$ for three hours. A pressure release valve is included in the structure.

Sorption pumps do not effectively remove helium, neon and

hydrogen, but by using two pumps in a system, the inert gases can be swept into the first pump and valved off, leaving the second pump to reduce the pressure to ion pump starting conditions.

The pumping speed of flat-cathode diode ion pumps is pressure dependent (Fig. 2-1) and differs from one gas to another. Pumping speeds are low for helium and neon, and extremely low for argon (one per cent of the figure for nitrogen). These figures can be improved by the use of a slotted cathode in the pump, or by a triode ion pump.

The argon-instability of diode ion pumps is well known, and due to saturation of the cathode by argon ions. This causes thermal runaway in the pump, with desorption of argon and a rapid increase in pressure to about 10^{-4} torr. The high partial pressure of argon then produces a large amount of sputtering, and the argon atoms are buried deeply and permanently in the cathode surface. If a system is operating against an air leak this process will repeat, unless pressures below 10^{-7} torr are maintained.

Ion pumps can be outgassed by baking to 250°C while operating. They have a life of about 50,000 hours at 10^{-6} torr, but can be regenerated by baking to 400°C with the magnets removed, using sorption pumps to take up the gases released.
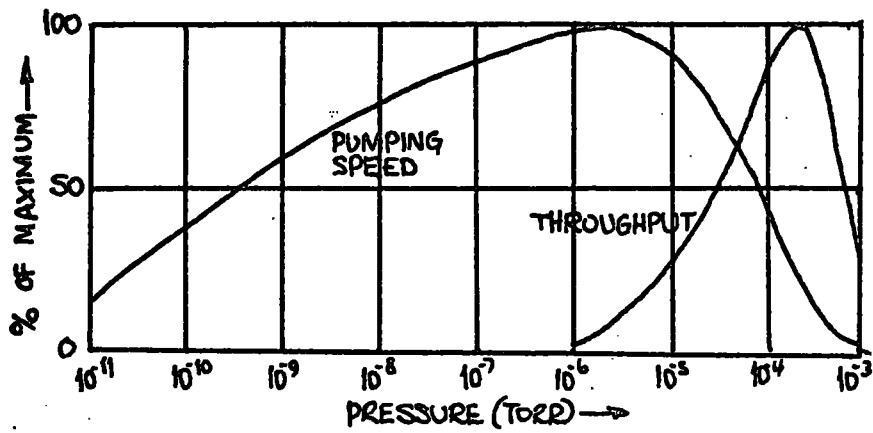
Fig. 2-1: Pressure dependence of the pumping speed and
throughput of a diode ion pump.

2-2 UHV system design

The inside height (nine inches) of the chamber designed and
built was defined by the size of the electron beam evaporator,
a substrate holder and an electron bombardment substrate heater.
The diameter was chosen as 11 inches, so that a standard 12 inch
bell jar could replace the stainless steel lid of the vessel.
The lid itself is sealed to the top flange by a viton ring or a
gold wire gasket. These considerations establish the volume
of the chamber at about 10 l, and its surface area at about
3,000 cm^2, including ports.

As the outgassing rate of unbaked electropolished stainless
steel is better than 10^{-9} torr l s^{-1} cm^{-2}, a pumping speed of
1.0 l s^{-1} for each 100 cm^2 of surface will produce pressures
better than 10^{-7} torr. A moderate bake to $150^{o}C$ would reduce
the outgassing rate to 10^{-11} torr l s^{-1} cm^{-2} and yield pressures
better than 10^{-9} torr. This figure is adequate for the work
contemplated. The speed of an ion pump falls to about 60 per cent
of its maximum at 10^{-9} torr, so a pump with a rated speed of
50 l s^{-1} is required. The Ferranti FJD80 ion pump, rated at
80 l s^{-1}, was selected to give some protection against system
leaks, electron gun outgassing and manufacturer's optimism.

A Vacuum Generators MSS50 sorption pump will rough an 8 l
system to 10^{-2} torr. Two of these pumps used in cascade will

handle 15 to 50 l with a changeover pressure of about 200 torr. It was decided to use two MSS50 pumps in the system, isolated from the chamber by an all metal bakeable valve (Vacuum Generators CR25) and two Edwards one-inch Speedivalves (see Fig. 2-2).

The stainless steel chamber was provided with four-inch ports using six-inch copper gasket flanges, for the ion pump and a window. One-and-a-half inch ports are provided in the base for mounting the electron beam evaporator assembly and in the lid for electrical feedthroughs (three-way 10kV 20A connectors) for the substrate heater. Other $1\frac{1}{2}$-inch ports in the side of the chamber accommodate an eight-way instrumentation feedthrough for thermocouples, a three-way 10kV 20A feedthrough for the evaporator supplies, and the roughing line. A two-inch port houses a nude Mullard IOG-13 ion gauge. Three blank $1\frac{1}{2}$-inch flanges are provided for accessories such as a leak valve, titanium sublimation pump, or shutter controls. The roughing line includes an air admittance valve and a Pirani gauge head.

The uhv system, with the exception of the roughing line, is mounted on a half-inch sheet of Sindanyo, a hard asbestos material. A bake-out heater, based on four 850W heater elements, was built for lowering onto the chamber or the ion pump for outgassing purposes. The heater case is made of Sindanyo lined with $\frac{29}{32}$-inch Viceroy insulation (a laminate of corrugated asbestos
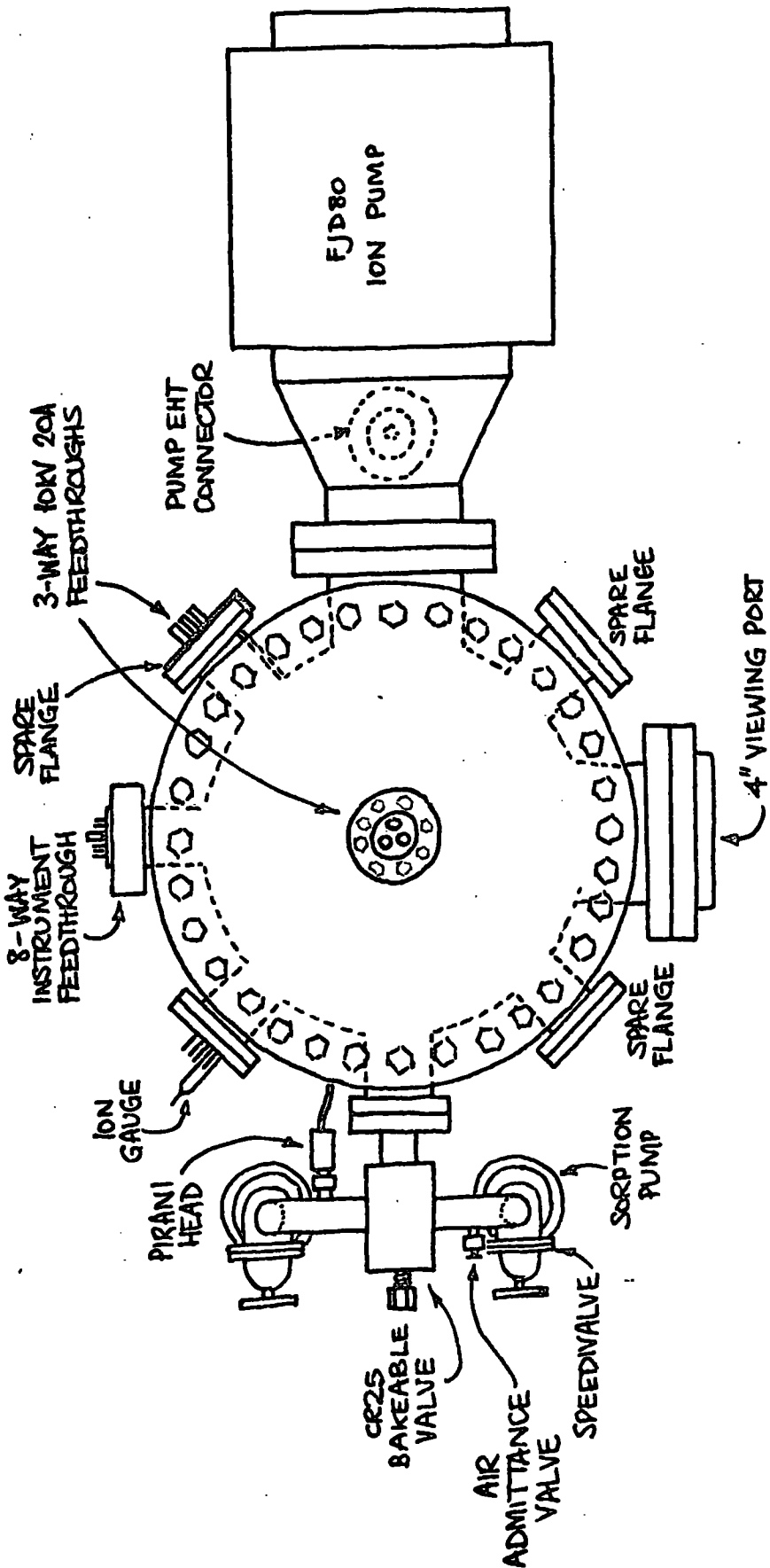
9.

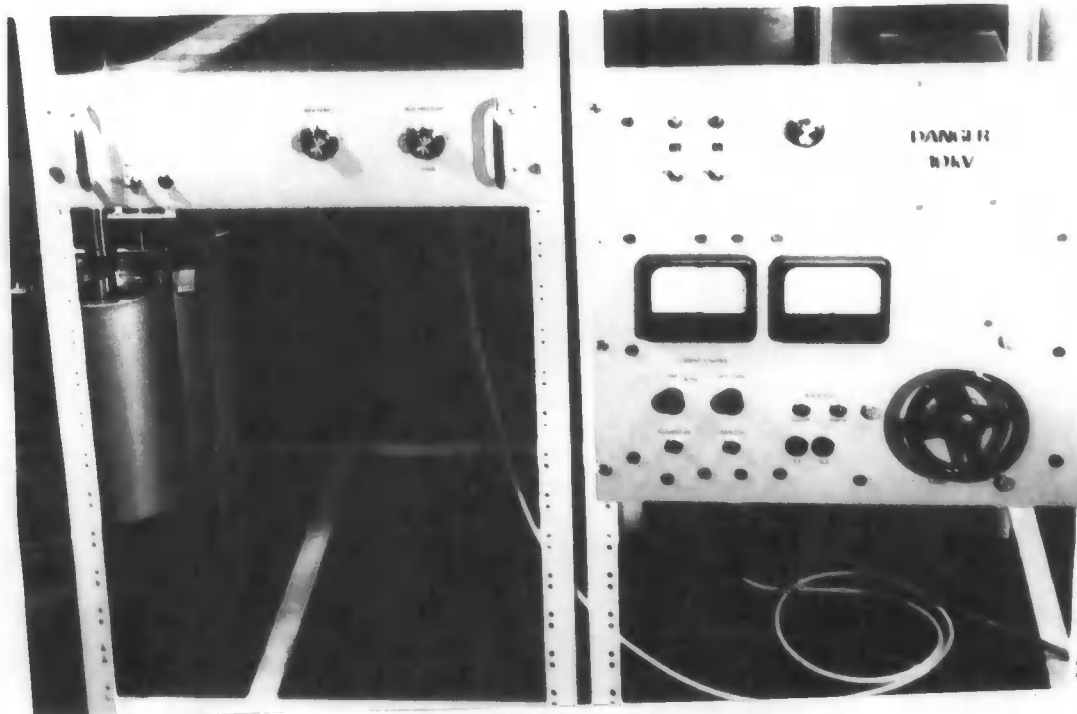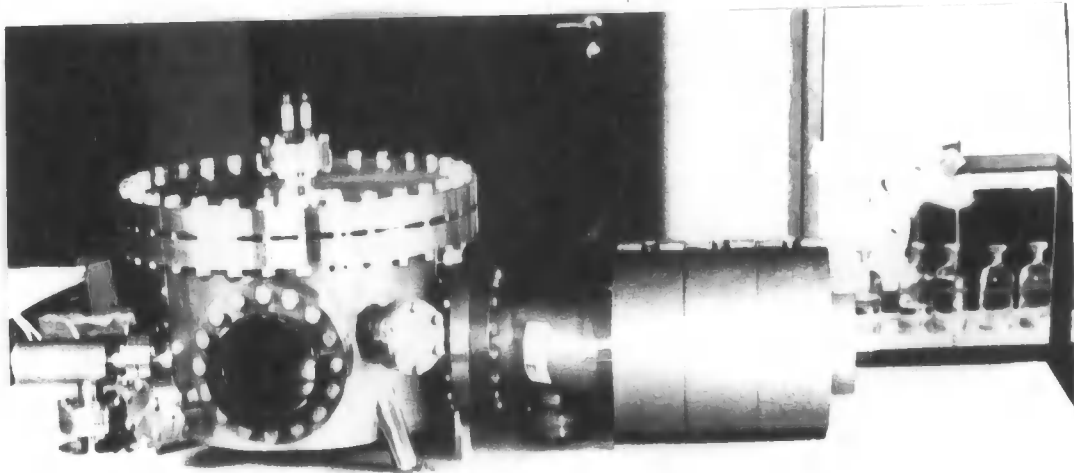Fig. 2-2: Plan of the uhv chamber, showing ports and the three pumps.

Plate 2-1: The uhv system, with the ion pump (right) and
sorption pumps (lower left). The electron beam evaporator
power supply (lower right) and bake-out control unit
(below the chamber) are also shown.

paper and flat aluminium foil by Bell's Asbestos and Engineering Limited). A bake-out control unit was designed and built, and is described in Section 2-4.

2-3 Ion pump power supply

The Ferranti FJD80 ion pump requires a power supply providing an open circuit voltage of 7.3kV and a short-circuit current of 200mA. This special feature is provided by a power transformer with a controlled high leakage inductance, which was obtained from Vacuum Generators Limited. The complete power unit provides protection against excessive pump current and metering of pump voltage, pump current and pressure (logarithmic scale). A control line is also provided for automatic switching of the heater used for the bake-out of the chamber or ion pump.

The circuit was developed from a commercial ion pump supply and has been found to function correctly over long periods of time.

The secondary voltage of the main power transformer (5.16kV rms off load) is rectified by a bridge circuit using 12 Lucas DD058 silicon diodes in each arm (Fig. 2-4). Each diode is paralleled with a 390kΩ resistance to ensure correct voltage sharing under reverse bias conditions. Smoothing is provided by a 0.5μF/10kV paper capacitor. Relay B switches the transformer primary circuit, and is made self-latching by contacts B1. The
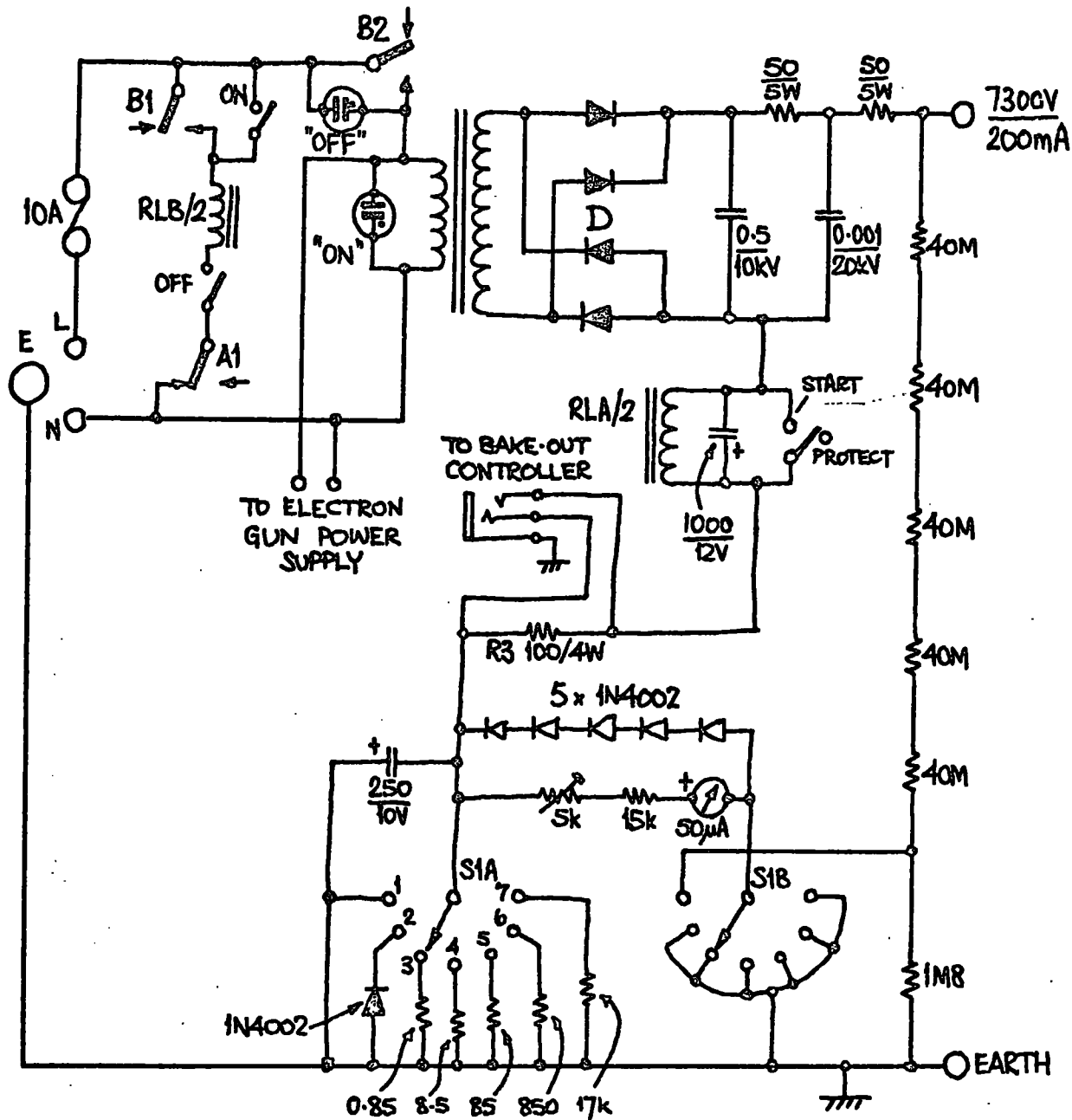
S1 FUNCTIONS

1. 10kV FSD
2. TORR ($10^{-9} - 10^{-4}$)
3. 1A FSD
4. 100 mA
5. 10 mA
6. 1 mA
7. 100 µA

RESISTANCE IN OHMS: CAPACITANCE IN MICROFARADS, UNLESS OTHERWISE STATED. BRIDGE RECTIFIER D HAS 12 OFF LUCAS DD058 DIODES IN PARALLEL WITH 390kΩ, IN EACH ARM.

Fig. 2-4: The ion pump power supply.

power supply is shut down by the OFF switch or by contacts A1

on relay A, which is energised if the pump current exceeds about

20mA, corresponding to a pressure of about $1.5.10^{-5}$ torr. The

START/PROTECT switch makes relay A inoperative while starting

the ion pump, when currents up to 200mA are permissible.

Leads are brought out from the transformer primary circuit

for use in controlling the electron beam evaporator supply

(Section 3-2), so that excessive chamber pressure causes automatic

shut down of all high voltage systems. Further, the voltage

developed across the 100Ω resistor R_1 by the pump current is

used to control the bake-out heater supply (Section 2-4), so that

a maximum chamber pressure is established during baking.

The meter circuit is based on a 50μA movement, and uses

conventional shunts to provide current ranges of 0.1, 1, 10, 100

and 1000 mA. Five 40MΩ high stability resistors are used in series

as a multiplier on the 10kV range. The pressure range, calibrated

from 10^{-9} to 10^{-4} torr, is based on the known relationship

between ion pump current and pressure, and an approximately

logarithmic scale is obtained by exploiting the properties of a

p-n junction diode.

The forward voltage drop across a p-n junction diode is

related to the diode current according to:

$$I = I_s (e^{eV/kT} - 1) \qquad \cdots (2\text{-}1)$$

where the symbols have their usual meaning. Measurements on a
sample of Texas Instruments 1N4002 diodes [2] have shown good
logarithmic properties over the current range 5nA to 1A, of the
form:

$$V = 100 \log_{10} I + 530 \qquad \cdots (2\text{-}2)$$

where I is in mA and V in mV (see Fig. 2-5).

The voltage across diode D5 is related to the pump current
in this manner and the 50μA meter is connected as a voltmeter
with a full scale sensitivity of 850mV, corresponding to a diode
current of 200mA. It is calibrated using the experimental graph
in Fig. 2-6 and the pump characteristic (Fig. 2-7). A true log
scale is obtained over the range 2.10^{-4} to 10^{-7} torr, but as the
diode current reduces and becomes comparable to the meter current
the scale loses its logarithmic form, and consequently provides
an expanded scale between 10^{-7} and 10^{-9} torr.

The meter is protected against current surges on all ranges
by diodes D6-D10.

The eht supply is coupled to the ion pump via high voltage
cable and a specially constructed brass/pyrophyllite high-temperature
connector.

2-4 Bake-out control unit

The bake-out heater consists of four 850W heater elements,
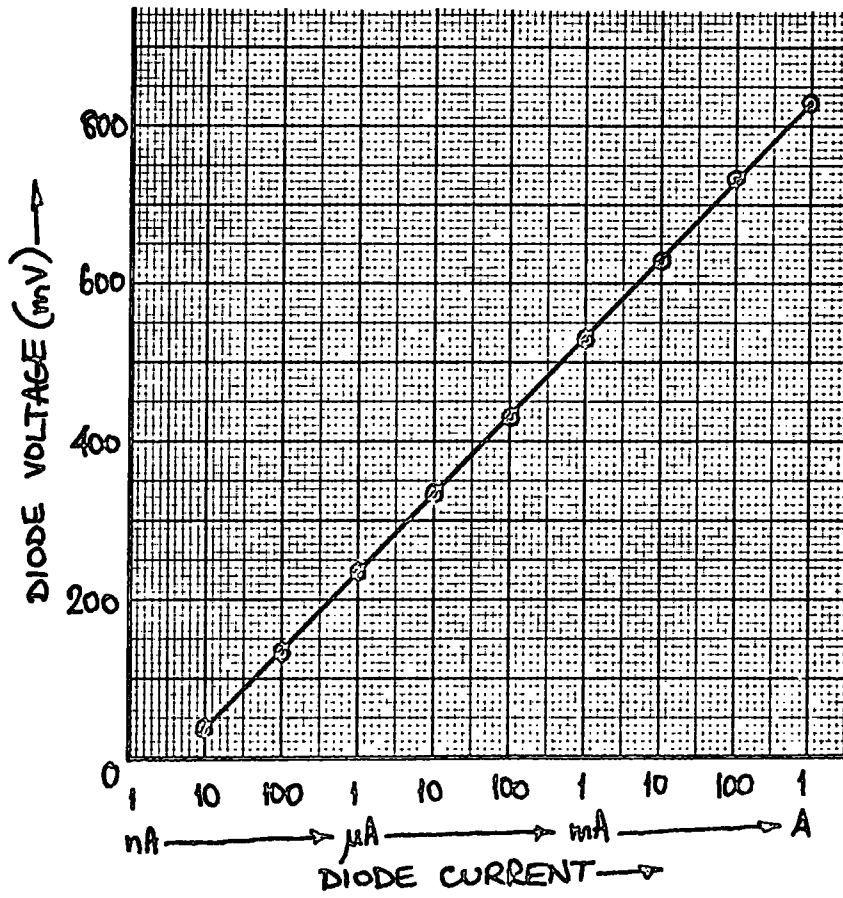
Fig. 2-5: The forward voltage drop across a Texas 1N4002 silicon diode plotted against diode current. (After Martin [2]).
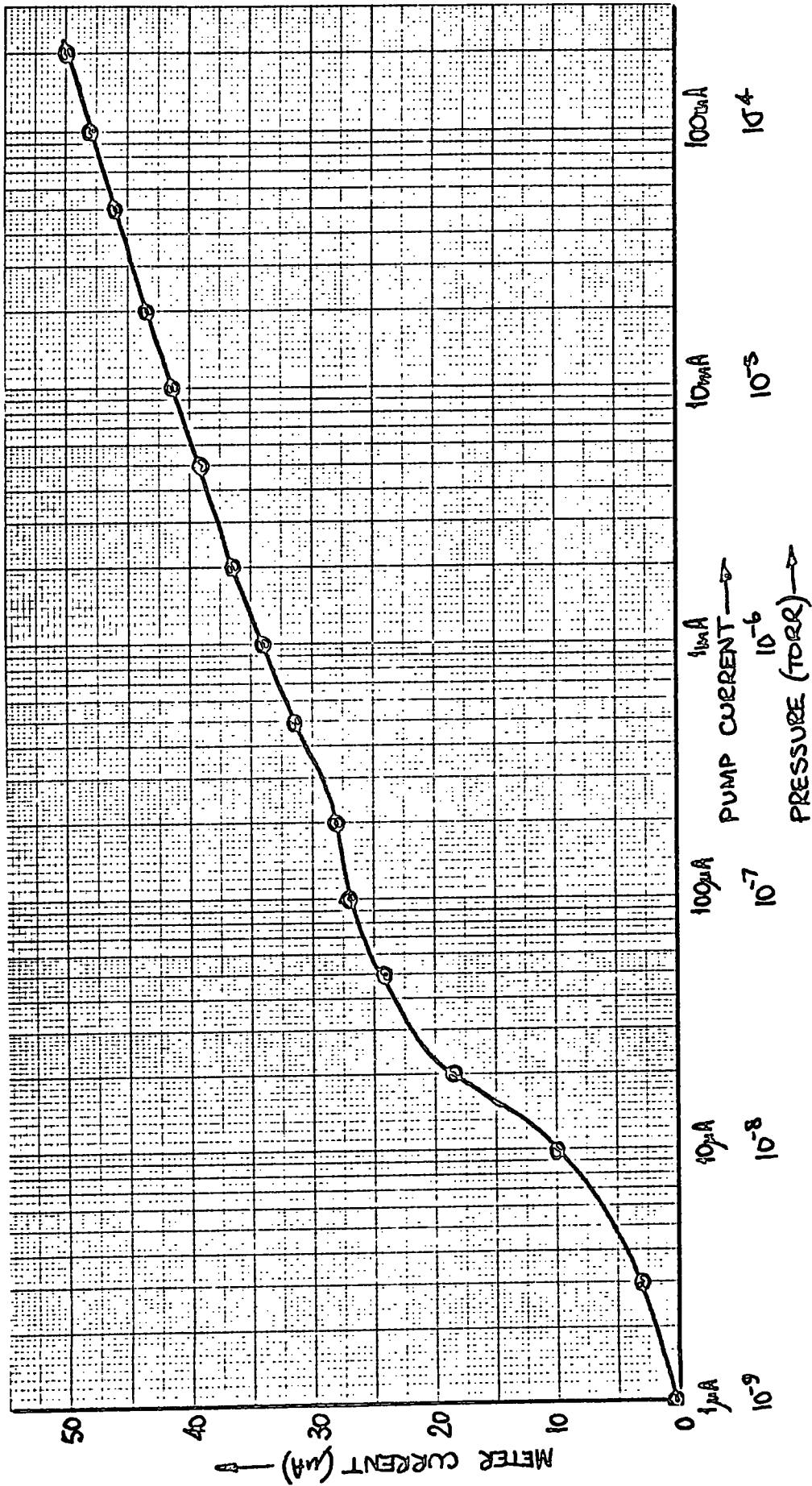
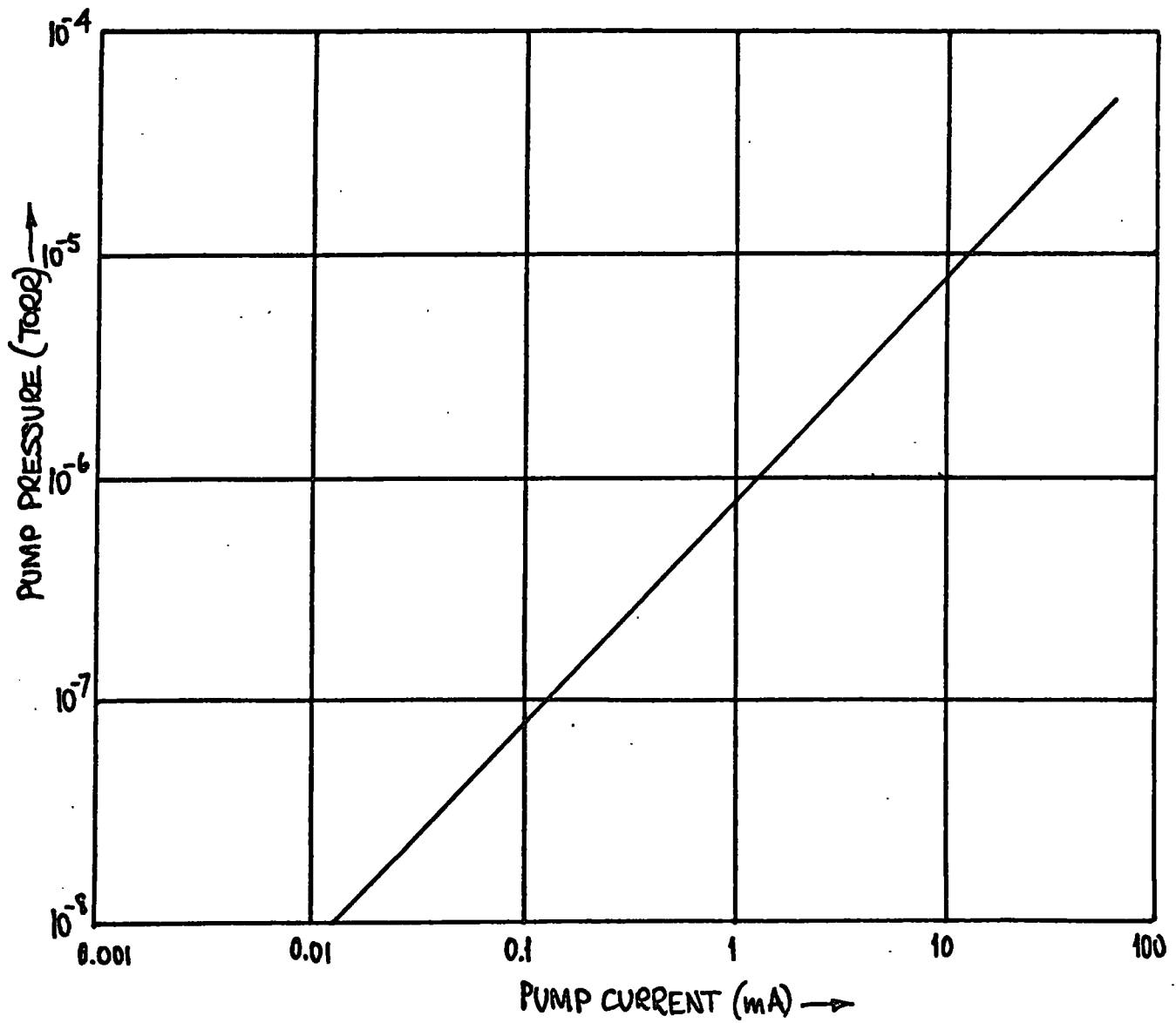Fig. 2-6: Characteristic of the logarithmic converter.

Fig. 2-7:   Ferranti FJD80 ion pump characteristic.

intended to be connected in parallel and driven by a 20A thyristor control unit. Control circuitry was designed to establish the maximum bake-out temperature and maximum chamber pressure.

The controller circuit developed, shown in Fig. 2-8, is based on a bridge-connected RCA 2N3872 thyristor gated by a simple unijunction trigger circuit. High current diodes (International Rectifier 16F60 and 16FR60) form the bridge circuit.

The unijunction fires the thyristor at some point on each half-cycle of the input waveform, the phase delay being determined by the time constant $C(R1 + P1)$. P1 establishes the mean heater current, and therefore the ultimate chamber temperature. If during baking the ion pump current exceeds a value determined by potentiometer P2, transistor Q1 conducts and relay A disables the unijunction trigger circuit. The critical pump current is variable from 10 to 60mA (10^{-5} to 6.10^{-5} torr). It is recommended that the lower limit is used in practice (see Section 2-5).

2-5 UHV system performance

After assembly the uhv system was roughed down to 10^{-2} torr in about five minutes, using the two sorption pumps in cascade. The ion pump was started, and on reaching 10^{-4} torr the roughing line was isolated by the high vacuum valve. An ultimate pressure of
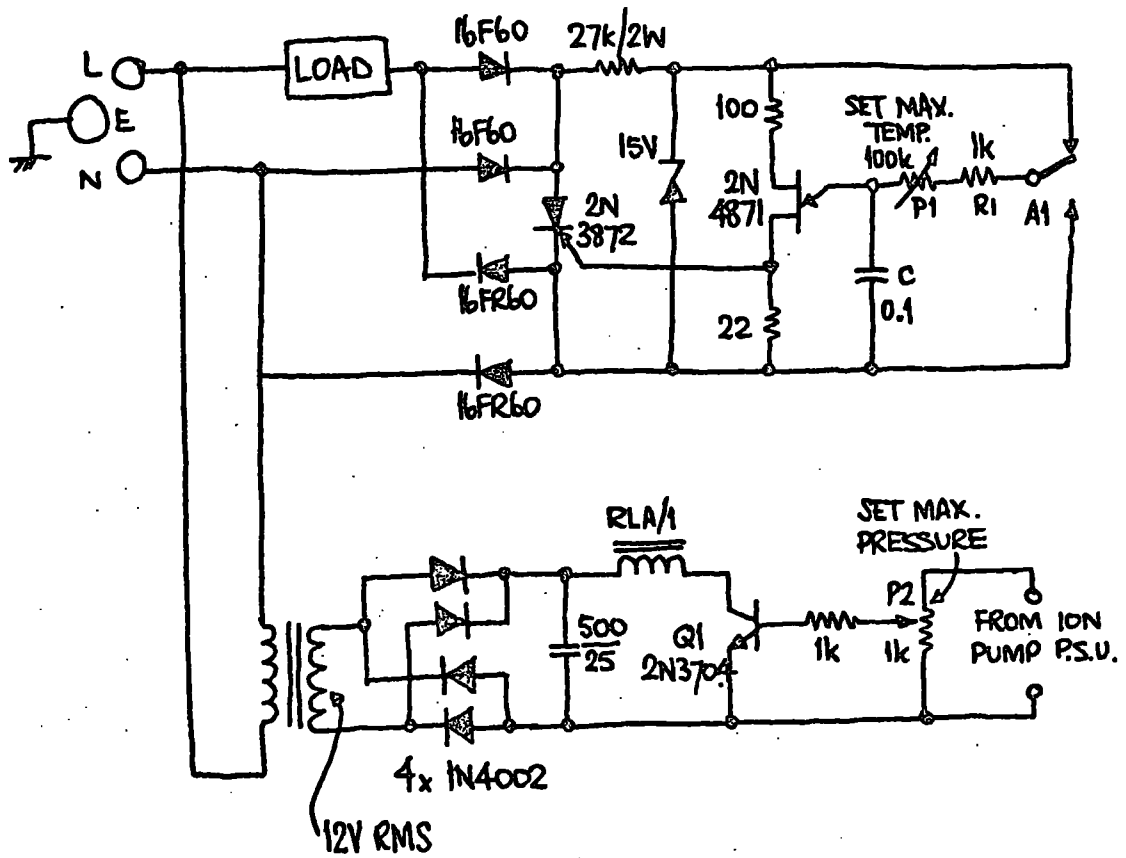
Fig. 2-8: Circuit diagram of the bake-out control unit.
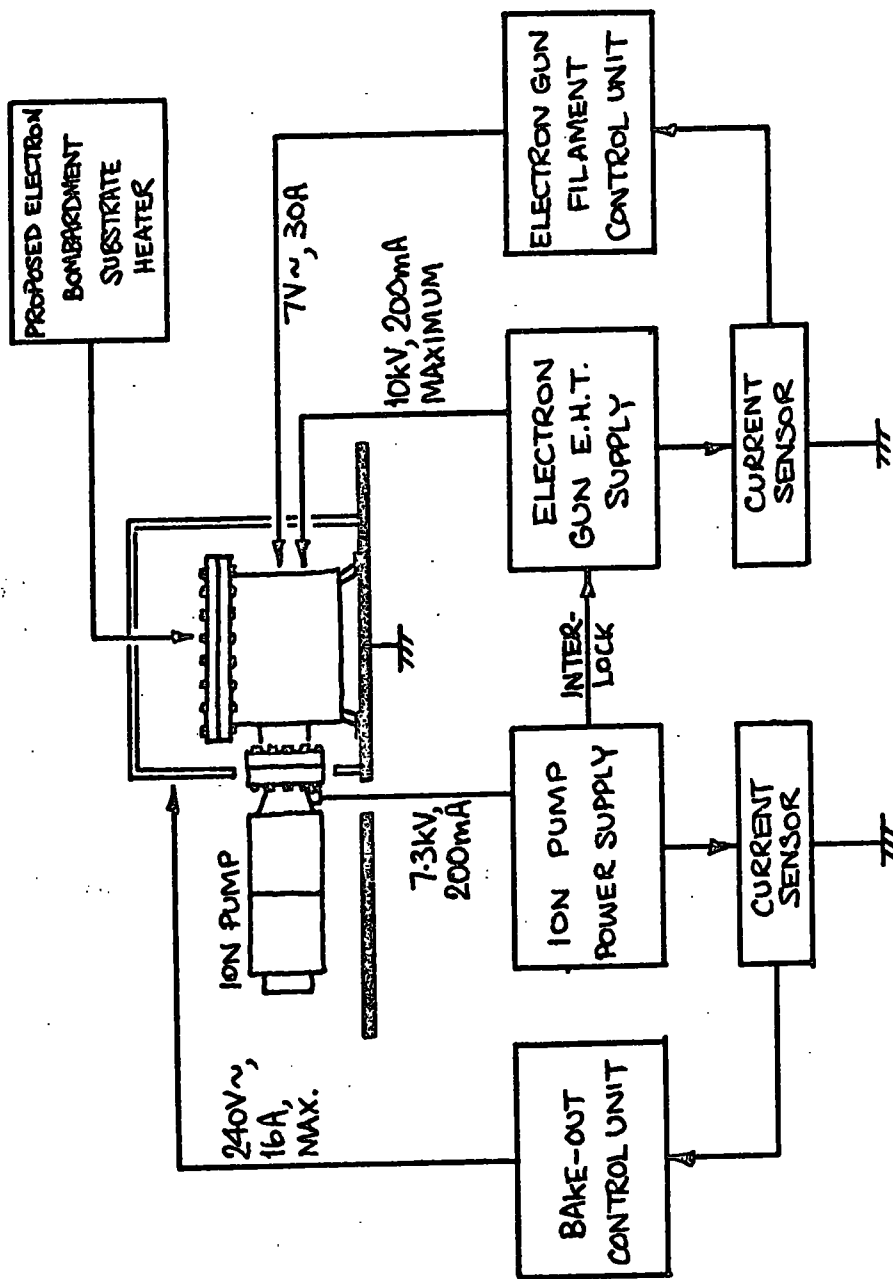
Fig. 2-9: UHV electronic systems.

5.10^{-7} torr was achieved after 20 minutes. Ion gauge measurements showed that the chamber pressure was identical to the pump pressure within the limits of experimental error.

Lower pressures were obtained by baking the chamber. The bake-out control unit was set to stabilise the chamber pressure at 10^{-5} torr, and a two-hour bake at 60°C yielded 2.10^{-7} torr on cooling. A further two-hour bake at about 80°C reduced the ultimate pressure to 5.10^{-8} torr. A final 50-hour bake to 180°C improved this figure to 1.10^{-8} torr on cooling. This pressure was confirmed by ion gauge measurements, and the leak rate measured as 1.4×10^{-5} lusecs. This figure is open to improvement but is within the capabilities of the pump. It is considered that a bake to $250-300^{\circ}$C would reduce the ultimate pressure a further order of magnitude.

It was found that if the bake-out procedure was carried out much above 10^{-5} torr the ion pump suffered from thermal runaway and the roughing line had to be used to restart the pump.

- Chapter 3 -

ELECTRON BEAM EVAPORATOR

3-1 The electron gun assembly

The electron gun is rapidly becoming one of the standard tools of the vacuum engineer, and is no longer used only for such specialist functions as vacuum welding and machining. Its usefulness rests with the properties of the electron beam: it is a clean method of heating and the beam can be directed to the spot where heating is needed. Combined with an ulra-high vacuum system, an electron gun is capable of producing a wide range of thin films with extremely low impurity levels. An electron bombardment substrate heater is frequently included in such systems.

The equipment designed and built for the fabrication of thin-films of willemite on silicon consists of:

(a) a clean uhv system based on a stainless steel chamber with sorption and ion pumps (Section 2-1);

(b) an electron beam evaporator; and

(c) provision for an electron bombardment substrate heater.

In 1965 Wales [3] described an electron beam evaporator for silicon and observed that the focussing of the gun was a

"very sensitive function of geometry". More recently Genevac
Limited and Vacuum Generators have manufactured complete gun
assemblies based on the same structure. The Genevac evaporator
is of the multiple hearth type and is therefore useful when
several successive layers of materials must be deposited, but it
is not specifically designed for use in uhv systems. The
Vacuum Generators gun is largely made of stainless steel, and
is mounted on a copper gasket flange. It is intended for use
in uhv equipment, and was chosen for the willemite work.

The Vacuum Generators EG1 electron gun is based on an
electrostatically focussed thermionic diode with a water cooled
anode hearth to hold the evaporant. The gun is constructed of
stainless steel, tungsten, molybdenum, nickel and a minimum of
ceramic. The whole structure (Fig. 3-1) is bakeable to 400°C.
In operation temperatures up to 3700°C can be achieved, with the
molten part of the evaporant supported on unevaporated material,
so preventing contamination from the hearth. Contamination is
further reduced by optically shielding the tungsten filament
from the substrate and evaporant. Focussing is variable, with a
range of spot sizes from one to seven mm.

During evaporation the gun operates with the filament and
cage below earth potential (up to -10kV, 200mA) and the hearth
is earthed. An emission-stabilised filament supply provides up
to 6V 14A.
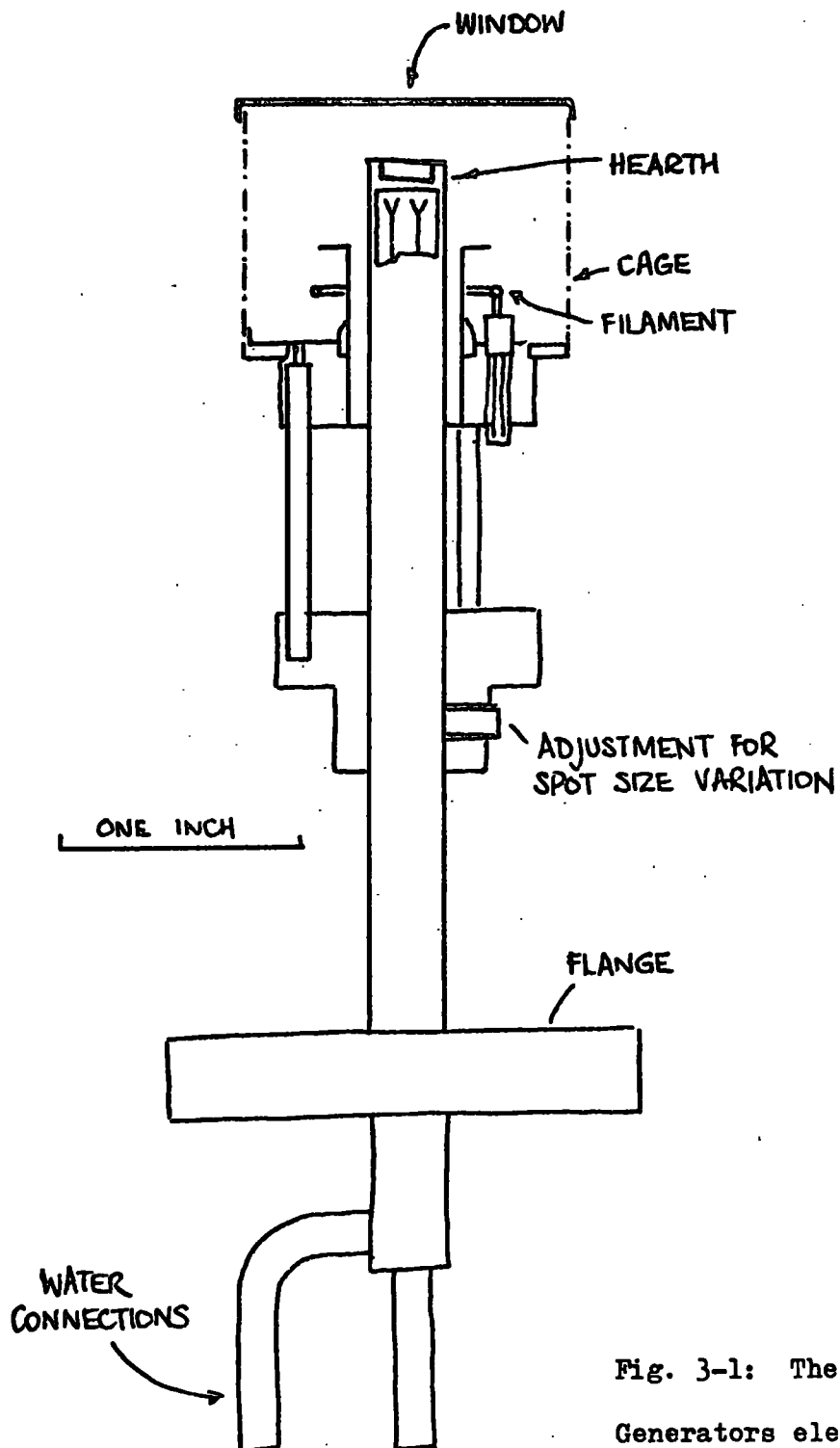
Fig. 3-1: The Vacuum Generators electron gun.

During degassing only the filament is held below earth potential (up to -2kV, 150mA). The gun structure temperature should not exceed 800°C.

Cooling water for the hearth is essential, and a flow rate of 30 gallons per hour is recommended by the manufacturers. The electron gun follows the three-halves power law, and Fig. 3-2 shows the emission current available with maximum permitted filament power.

To prepare films in a reasonably short time, the vapour pressure of the evaporant must be raised to at least 10 microns of mercury [4]. For metals the rate of evaporation (W) can be calculated from:

$$W = 5 \cdot 85 . 10^{-5} p . \frac{M}{T} \quad gm \ cm^{-2} \ s^{-1} \qquad \ldots (3-1)$$

where M is the gram-molecular weight, and p the vapour pressure in microns at a temperature T (°K). Table 3-1 gives the temperatures needed for vapour pressures of 10 microns with some common materials [4]:

Metal	Au	Al	Ge	Si
T(°C)	1465	996	1251	1343

Table 3-1.

3-2 Electron beam evaporator power supply

The power requirements for the Vacuum Generators EG1 electron gun
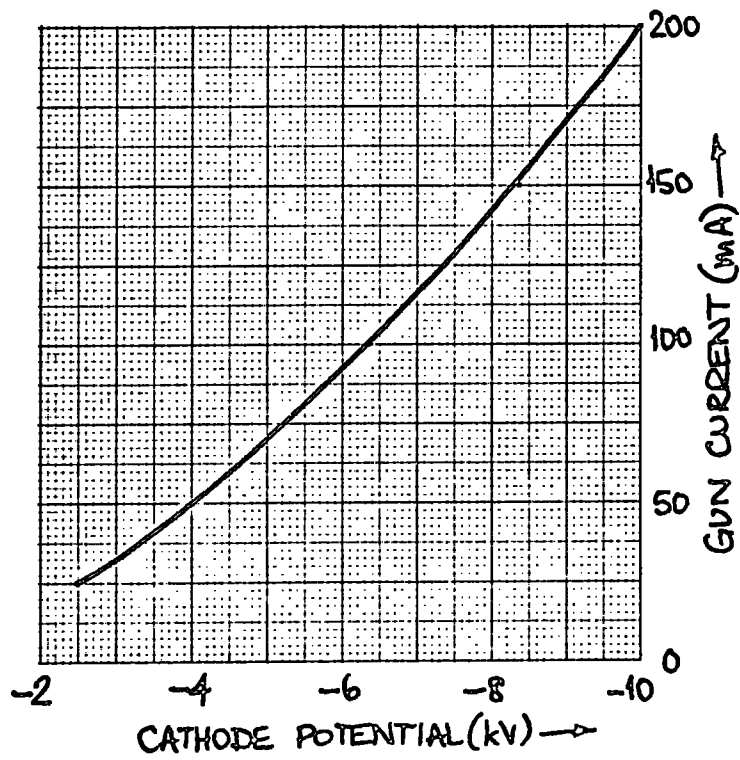
Fig. 3-2: Emission curve for the Vacuum Generators EG1
electron gun, at maximum rated filament power.

are:

(a) for evaporation, an eht supply of 0-10kV at up to 200mA
and a stabilised filament supply of up to 6V 14A, insulated
from ground to better than 10kV; and

(b) for outgassing, an eht supply of up to 2kV 150mA, and a
filament supply of 6V 14A.

In view of the high voltage and power levels involved,
various protection and interlock circuits are desirable. The
following features have been included in the power supply
design:

(a) a trip circuit to shut down the equipment in the event of
an overload or flashover;

(b) a microswitch coupled to the shaft of the Variac controlling
the main eht voltage to prevent turning on the supply without
first setting the eht to zero;

(c) an interlock switch to operate in the event of failure of the
hearth water supply;

(d) a protection circuit in the filament control system to protect
the filament from excessive current in the event of an
eht failure;

(e) a protection circuit to shut down the supply if the chamber
pressure exceeds 2.10^{-5} torr; and

(f) various devices, including diodes and an inductor, to

protect some power supply components from transient overloads.

As the electron gun is a thermionic diode, emission current
is highly dependent on filament current. It is therefore
desirable to use a feedback circuit to control the filament
current and maintain the anode current at a preset level. This
is a procedure commonly adopted in the design of thermionic diode
noise generators.

The eht transformer (Fig. 3-3) has a maximum output of
7.3kV rms, which after bridge rectification and smoothing provides
-10kV with a current capability of 200mA. The primary circuit
includes an 8A Variac and is controlled by various switches and
relay contacts.

Provided the water supply to the hearth is in order and the
Variac is set to zero, the ON switch will operate relay B (which
is self-latching), and supply power to the eht transformer.
The OUTGAS/EVAPORATE switch selects the appropriate cage voltage.
If the gun current exceeds 200mA relay A is energised and breaks
the transformer primary circuit by unlatching relay B.

Eht current is monitored by a 1mA meter, shunted to 200mA
fsd and protected by D4 (Motorola 1N4719). This diode was
selected for its high surge current rating of 600A for 1ms.
The gun current is also monitored by a 6V filament lamp which is
coupled to a cadmium sulphide photocell in the filament control
circuit. The lamp is protected by a 7·5V Zener diode (Mullard
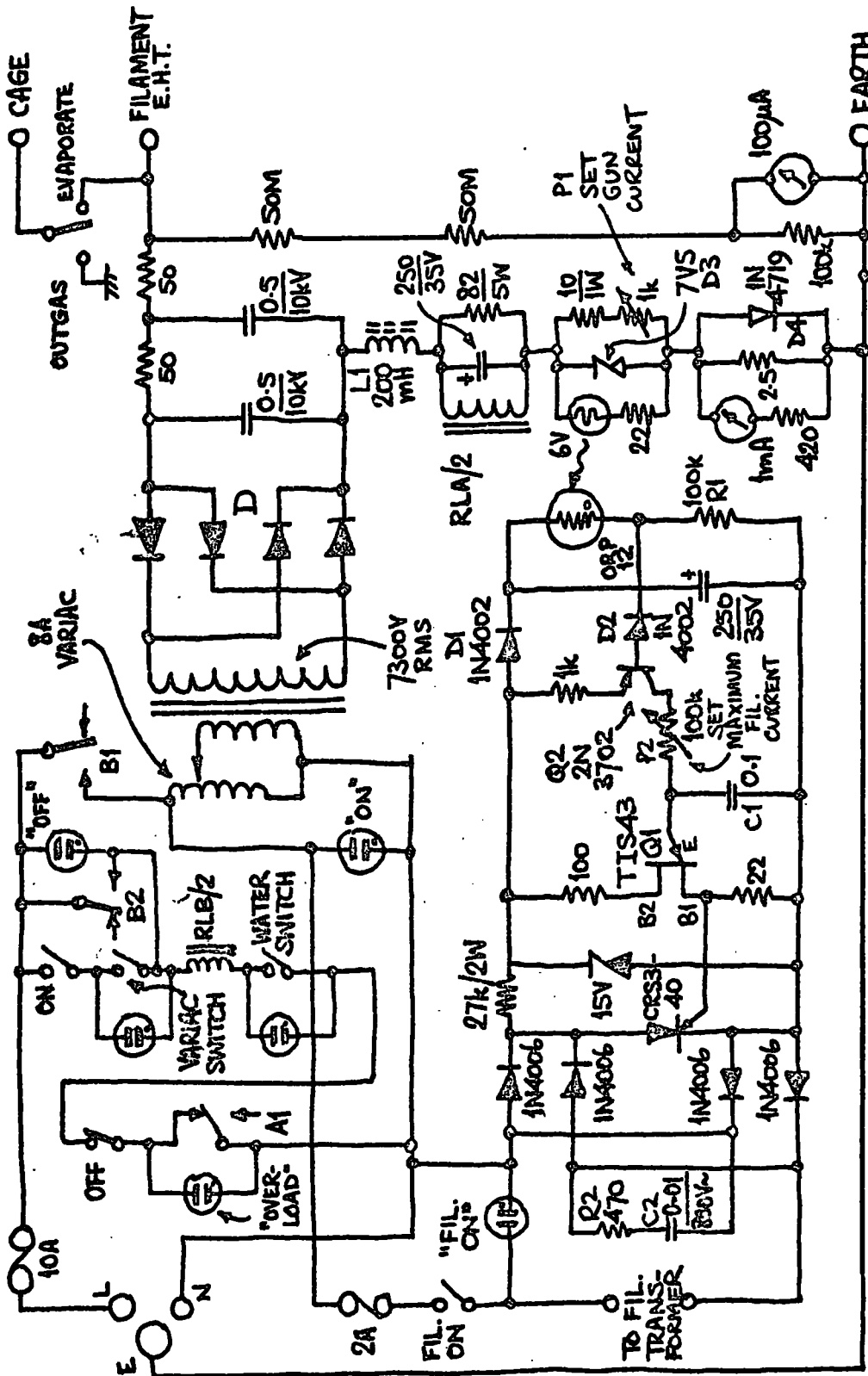
Fig. 3-3: Circuit diagram of the electron beam evaporator power
supply.

BZY93-C7V5), again with a high surge rating. In the event of an eht short circuit or heavy discharge, the current rise-time is increased by the 200mH inductor Ll. This limits the peak current to less than 25A: without Ll the initial short circuit current is over 100A.

The filament current is controlled by a bridge-connected unijunction-fired thyristor (STC CRS3-40) in the filament transformer primary circuit, in a circuit similar in principle to that designed for the bake-out controller (Section 2-4). Transistor Q2 in the unijunction emitter circuit is a constant current generator controlling the charging rate of the timing capacitor Cl. The ORP12 photoresistor and the 100kΩ resistor Rl provide a light-dependent voltage for the base of Q2. Diode D2 prevents reverse base-emitter breakdown in Q2. Potentiometer P2 is used to set the maximum charging rate in Cl, and hence establish a maximum filament current. The thyristor and its diode bridge are protected against voltage transients by the network C2-R2.

The optical coupling between circuits in the feedback loop was considered the simplest approach to the problem caused by 50Hz a-c voltages existing between the unijunction circuit and earth. An alternative approach would have been to use a insulated pulse transformer between the unijunction and the thyristor gate. In the circuit adopted there are two prominent time constants: the response time of the cadmium sulphide photocell (about 20s)

and the thermal time constant of the gun filament. If low frequency oscillations occur, it is necessary to artificially increase the photocell response time by means of a high value capacitor across Rl.

In common with the bake-out heater and control unit, and the ion pump supply, the electron gun supply is designed for unattended operation over long periods. All units are protected against faults in circuits or equipment. The evaporator and its power supply have been tested for correct operation, and are available for the production of new display devices.

- Chapter 4 -

THE C-V PLOTTER

4-1 Aims and applications

Grove [5] and others have shown that the electronic processes
associated with certain types of solid state devices can be
assessed quantitatively by measuring the dependence of device
capacitance on applied bias voltage. With simple p-n junctions
the behaviour of the depletion layer can be studied, and in
metal-insulator-semiconductor (MIS) structures data on surface
states, ion transport phenomena and other parameters becomes
available. The willemite display devices (MWS) developed in the
Department have been analysed by Edwards [1], using C-V
measurements obtained from the instrument described in this
Chapter.

The C-V Plotter developed for this work was intended for
use with devices which were almost purely capacitive: for most
work the effective parallel resistance must be greater than
about 100kΩ. This restriction does not affect measurements on
MOS or MWS structures, but the instrument is unable to measure,
for instance, the capacitance of a forward-biased p-n junction
diode, due to its high conductance.

In operation, the device capacitance forms part of the total

capacitance of an oscillator tuned circuit. Small changes in oscillator frequency caused by changes in device capacitance are detected by beating the oscillator output with an external signal source, and converting the varying beat frequency to a d-c voltage suitable for driving an X-Y recorder. The instrument includes a very low frequency sweep generator capable of biasing the device under test over the range -20 to +20V.

In drawing up a specification for the C-V Plotter, the important parameters are:

(a)   the range of device capacitance the instrument should be capable of measuring. It was decided to accommodate the range 1-50pF at all operating frequencies, although this figure can be considerably increased at low frequencies;

(b)   the a-c voltage superimposed on the swept bias voltage and applied to the device. This should be as small as possible so that the bias voltage is not significantly modulated by the signal voltage. A figure below about 50mV rms was considered satisfactory;

(c)   the swept bias voltage range. As it was not intended to study high-voltage devices with the Plotter, a swept bias voltage switchable between ±0.5 and ±20V was adopted;

(d)   the range of measurement frequencies. Although the inductance in the oscillator tuned circuit is fixed at 0.5mH, limiting

Plate 4-1: The C-V Plotter.

the frequency range of the instrument to 150-450kHz, a

front-panel switch is included so that further inductors

may be added and selected. Values of 0·5, 2, 10, 50, 200

and 1000mH are suggested, which would increase the

frequency range to 4kHz-450kHz.

4-2 <u>Circuit details</u>

The oscillator circuit is based on the Franklin configuration.

This has the advantage of using a simple parallel tuned circuit

with one end earthed, without the large feedback capacitors

associated with the Clapp-Gouriet or Colpitts circuits.

However, certain changes had to be made to reduce the sensitivity

of the Franklin oscillator to changes in tuned circuit Q caused

by device conductance, and to reduce the a-c signal appearing

across the device.

A conventional Franklin circuit for frequencies of the

order of 500kHz is shown in Fig. 4-1. It consists of a loosely-

coupled two-stage JFET amplifier with overall positive feedback

via the tuned circuit L1-C1. Coupling capacitors C2, C3 and C4

have small values, to minimise tuned circuit loading and reduce

overall loop gain, so improving the oscillator frequency stability.

The a-c voltage across the tuned circuit is large (of the order

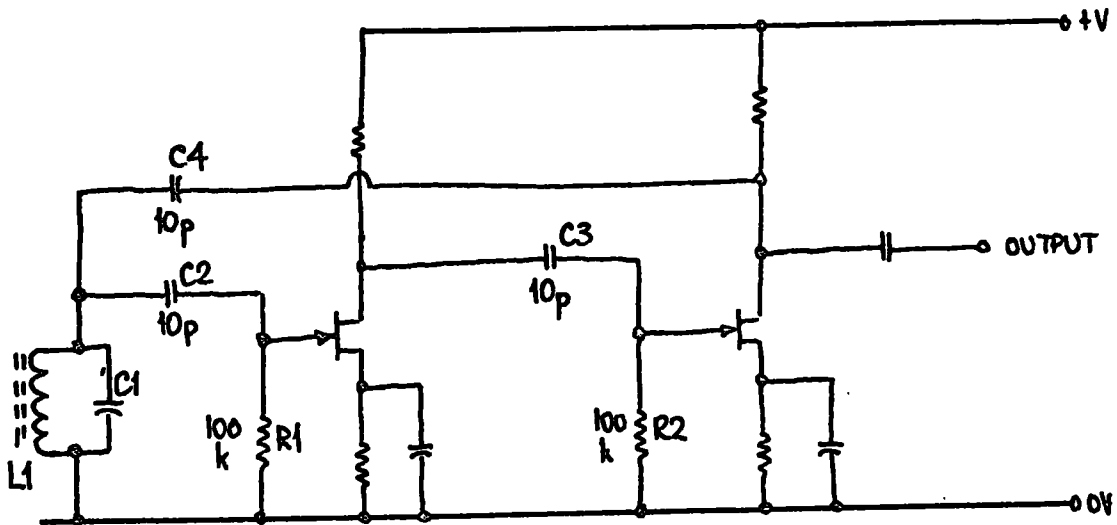of a volt), and too high for connection to devices under test.

Fig. 4-1: A conventional Franklin oscillator for frequencies of the order of 500kHz.

The small size of the coupling capacitors introduces three spurious phase-shifts into the feedback loop: those due to C2-R1, C3-R2 and C4 with the dynamic resistance of the tuned circuit, including the device under test. The circuit therefore does not oscillate at the true resonant frequency of the tuned circuit but at a nearby frequency where the overall loop phase-shift is 360°. This frequency error, due mainly to the smallness of C4, can be greatly reduced by using conventional coupling capacitors (0.01μF) and other means of reducing loop gain.

In the modified circuit (Q1 and Q2 in Fig. 4-2) the loop gain is set by the preset FEEDBACK potentiometer P1. Diode D1 limits the a-c voltage at the gate of Q2 to 200mV peak: this a.g.c. action limits the a-c voltage across the device to 30mV peak.

A 1600pF variable capacitor is provided to vary the operating frequency and instrument sensitivity. Large changes in frequency can be obtained by switching the tuned circuit inductance. The instrument is calibrated by fixed capacitors of 0, 10, 20, 30, 40 and 50pF which can be switched into the circuit.

Q3 is an emitter follower, isolating the oscillator from the diode mixer D2 and the external oscillator, and preventing phase-locking. After filtering, the audio frequency output of the mixer is amplified (Q4, Q5) and squared in a Schmitt trigger circuit (Q6, Q7). An emitter follower (Q8) provides a low source
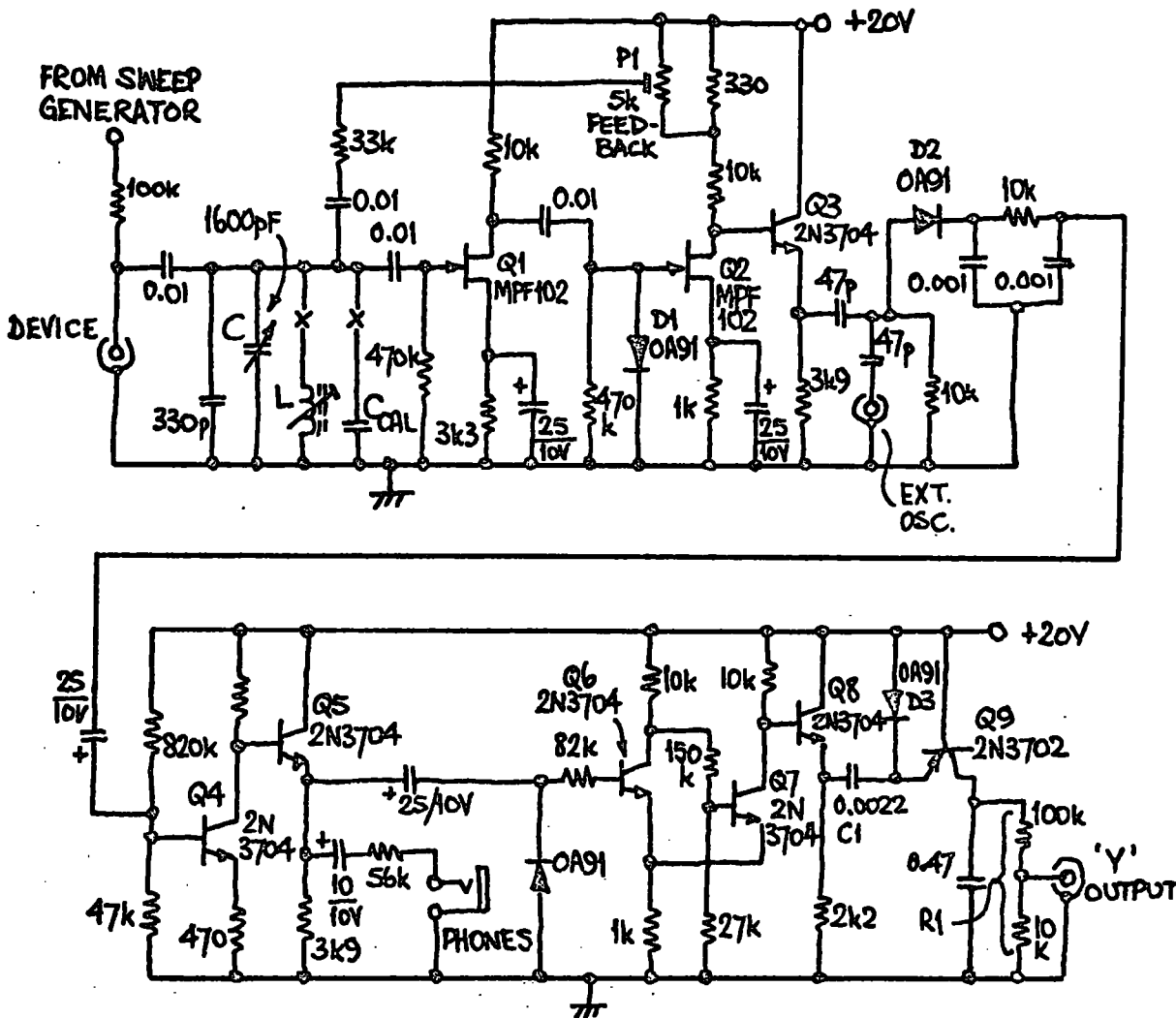
RESISTANCE IN OHMS, CAPACITANCE IN MICROFARADS, UNLESS OTHERWISE STATED. C_{CAL} IS SWITCHABLE FROM 0 TO 50PF IN STEPS OF 10PF. L IS SWITCHABLE TO VALUES OF 500uH, 2mH, 10mH, 50mH, 200mH AND 1H.

Fig. 4-2: Circuit diagram of the oscillator, mixer and

frequency-to-voltage converter in the C-V Plotter.

impedance for the diode-transistor pump (D3, Q9) which is used as a highly linear frequency-to-voltage converter, with the law:

$$V = fC_1R_1V_{in} \qquad \ldots (4\text{-}1)$$

where V_{in} is the amplitude of the input square-wave signal with a frequency f.

The Y-output of the instrument is derived from the d-c output voltage of the pump circuit. The beat frequency can be monitored on headphones connected to the emitter of Q5.

The complete sweep generator circuit is shown in Fig. 4-3. The Plessey SL701C integrated circuit operational amplifier is connected as an integrator generating a ramp voltage with a slope depending on its input voltage, set by the SPEED control P1. A Schmitt trigger circuit (Q1, Q2) detects when the integrator output crosses definite upper and lower voltage levels, and reverses the polarity of the integrator input voltage. Potentiometer P5 sets the symmetry of the triangular wave generated in this way.

The integrator output is amplified in a specially designed complementary circuit (Q4, Q5, Q6, Q7) with overall negative feedback (R1, R2) to define the gain. High frequency stabilisation is provided by the 330pF capacitors between base and collector of Q6 and Q7. The output of this amplifier is bipolar, and
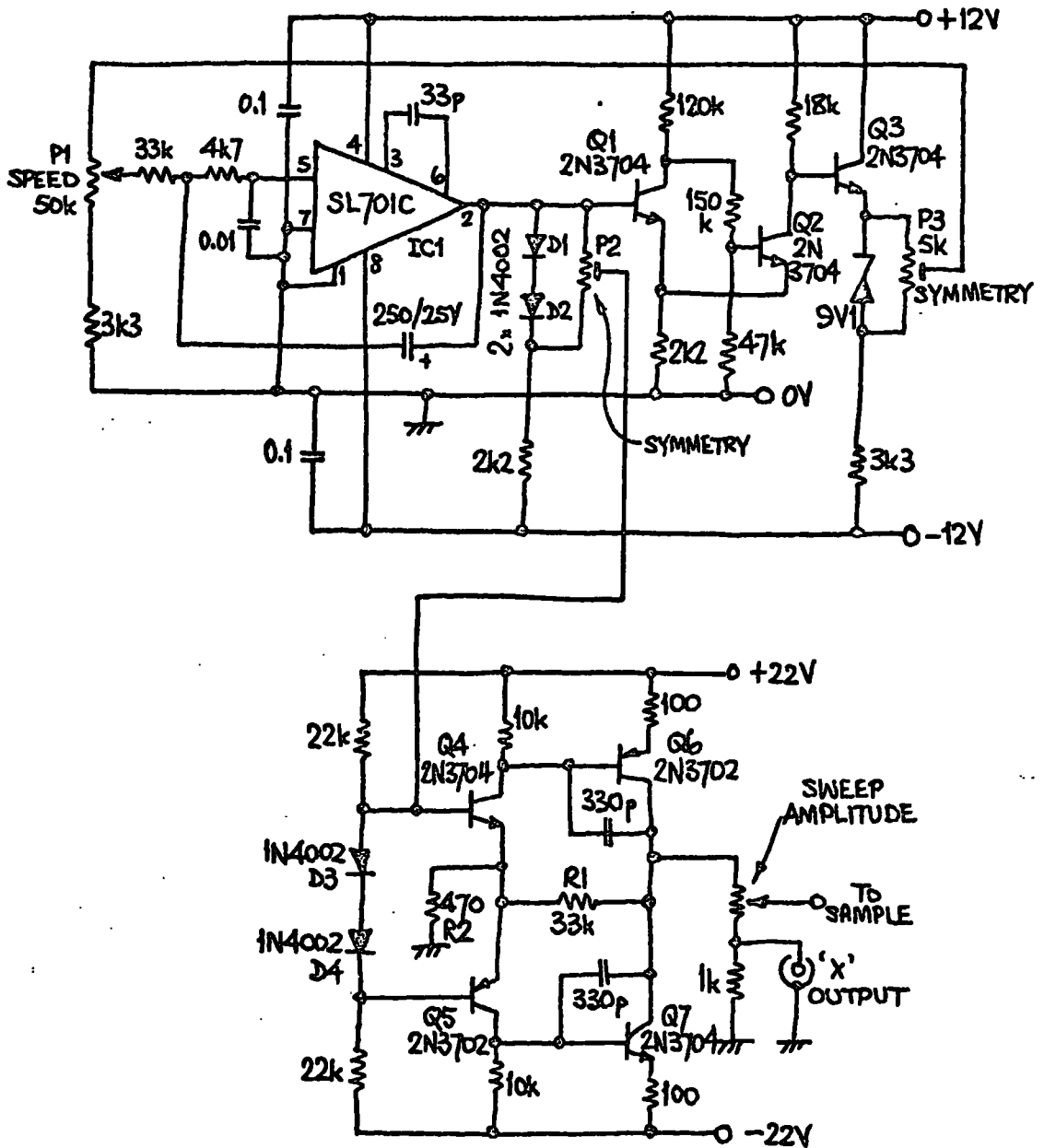
RESISTANCE IN OHMS, CAPACITANCE IN MICROFARADS, UNLESS OTHERWISE STATED.
SWEEP AMPLITUDE SWITCHABLE TO ±20V.

Fig. 4-3: Circuit diagram of the C-V Plotter sweep generator.

switchable between ±0·5 and ±20V. Diodes D1 and D2 provide a d-c offset to restore the integrator output waveform to symmetry about earth potential. The current through diodes D3 and D4 determines the quiescent current in the amplifier output transistors.

The amplifier is deliberately overdriven into symmetrical clipping so that the sweep voltage waveform is a slightly truncated triangular wave. In this way, the pen of the X-Y recorder used with the C-V Plotter is made stationary for a moment after each complete sweep. This facilitates raising and lowering the pen at the correct point. The feedback resistor R1 was selected so that this condition was achieved. The period of the sweep voltage waveform is variable between about 4 seconds and 2 minutes.

The C-V Plotter power supply provides four voltages: -22, -12, +12 and +22V. Fig. 4-4 shows the conventional regulator circuits used for each supply.

4-3 Results and limitations

The C-V Plotter has been used for the assessment of MWS display devices [1], for studying some properties of MOS transistors and for other work in the Department.

The instrument is normally used at frequencies around
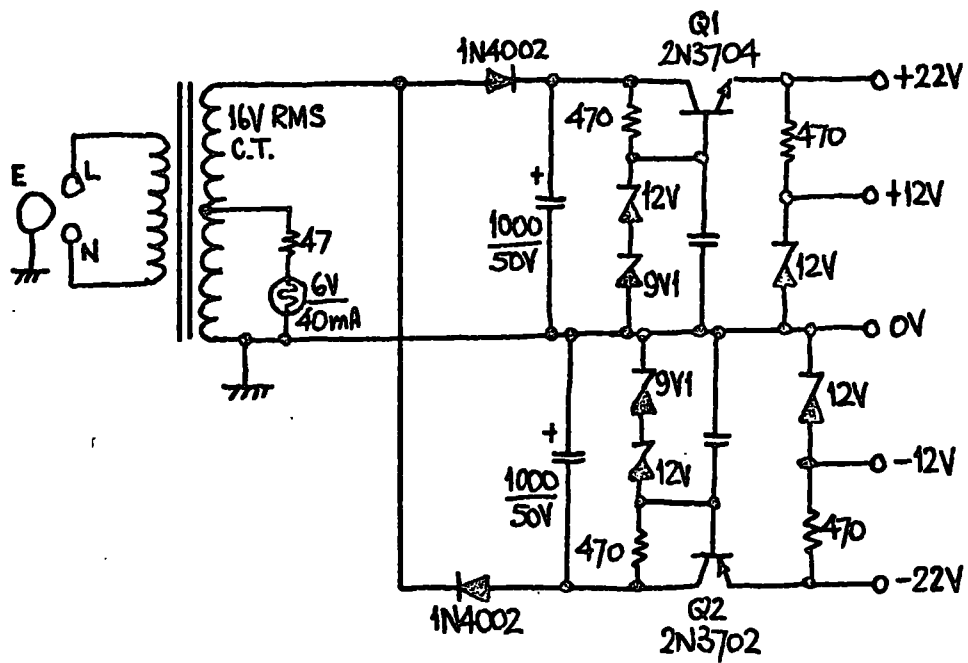
RESISTANCE IN OHMS, CAPACITANCE IN µF, UNLESS OTHERWISE STATED.

Fig. 4-4:   The C-V Plotter power supply.

300kHz and will readily resolve changes in capacitance of 0·1pF. With care this figure can be improved to about 0·01pF, but it is important that device conductance should be low, certainly less than 0·1μ℧, when working to such accuracy. Even higher sensitivity should be possible by beating the external oscillator with a harmonic of the internal oscillator.

The effects of device conductance on accuracy have been investigated, and the results are shown in Fig. 4-5 expressed as an equivalent capacitance change at an operating frequency of 200kHz (total circuit capacitance 1000pF). The graph has a constant slope of 0·1pF μ℧$^{-1}$.

The simple C-V Plotter has two distinct limitations:

(a) the inability to measure device capacitance and conductance separately; and

(b) the inability, in the present design, to measure the capacitance associated with large area display devices. The maximum resolvable capacitance is restricted by the mixer bandwidth and the range of the frequency-voltage converter to just over 50pF, at operating frequencies of 200-300kHz.

The conductance-capacitance (G-C-V) Plotter described in Chapter 5 is capable of measuring conductance and capacitance over a wide range of values and test frequencies.
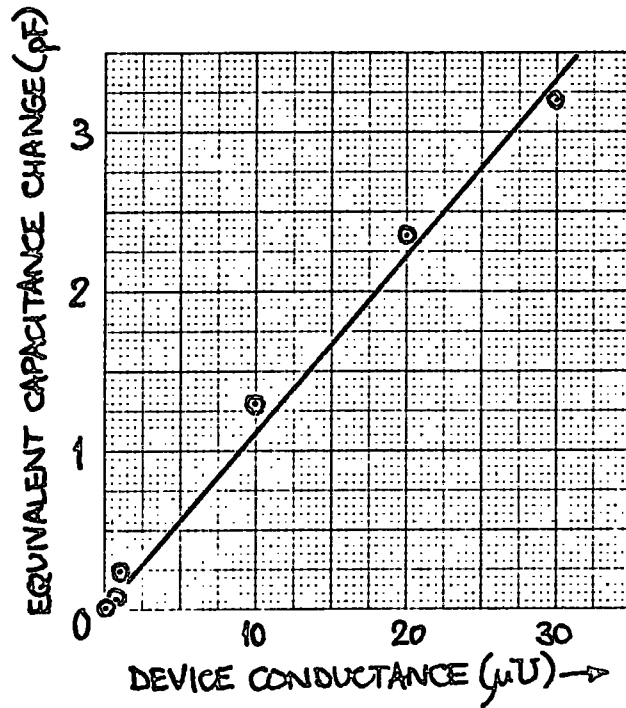
Fig. 4-5: Graph showing the effects of device conductance on C-V Plotter accuracy, expressed as an equivalent capacitance change.

- Chapter 5 -

THE CONDUCTANCE-CAPACITANCE PLOTTER

5-1 Introduction

The usefulness of C-V measurements in the assessment of solid-
state devices is well-established, but more recently the use
of a-c conductance measurements has also been exploited. The
G-C-V (conductance and capacitance versus voltage) Plotter to
be described is capable of measuring both functions simultaneously
and over a wide range of values and test frequencies. Other
workers [6] have built instruments based on similar principles
to those adopted here, but with less versatility and a lower
dynamic range.

Section 5-2 discusses previous work, and a specification
is drawn up in Section 5-3. The subsequent parts describe circuit
design and results.

5-2 Survey of previous work

The instability of some semiconductor devices has long been
attributed to the motion of ions in the strong electric fields
where a p-n junction intercepts the surface of a device. With
planar processes this problem has largely disappeared for bipolar

transistors, but MOS devices are sensitive to ion motion in the oxide layer. C-V measurements can be used to study ion transport properties in MIS and other structures, and this work is of considerable importance.

A wide range of experimental results from C-V measurements on MOS devices has been published by Grove et al [5]. Fig. 5-1 shows the general form of the curves obtained. Under negative bias, the device capacitance equals the oxide layer capacitance (C_0), as no space charge / exists in series with it. Under forward bias, depletion occurs in the silicon, causing a steady reduction in capacitance. However, minority carriers are created, and at low measuring frequencies these have sufficient mobility to follow the applied signal and contribute to the device capacitance. At high frequencies the minority carriers are not sufficiently mobile, and majority carriers create a space-charge which gives a constant device capacitance at positive bias. The depletion case is only seen if the oxide layer is leaky or if the d-c bias is switched on so rapidly that the capacitance is measured before minority carriers accumulate near the surface.

Fig. 5-2(a) shows the effect on C-V curves of surface states with positive charge, and Figs. 5-2(b) and (c) show the dependence on doping levels in the silicon and on the thickness of the oxide layer. Energy in the form of heat or light incident on the device increases the number of minority carriers and gives rise to effects
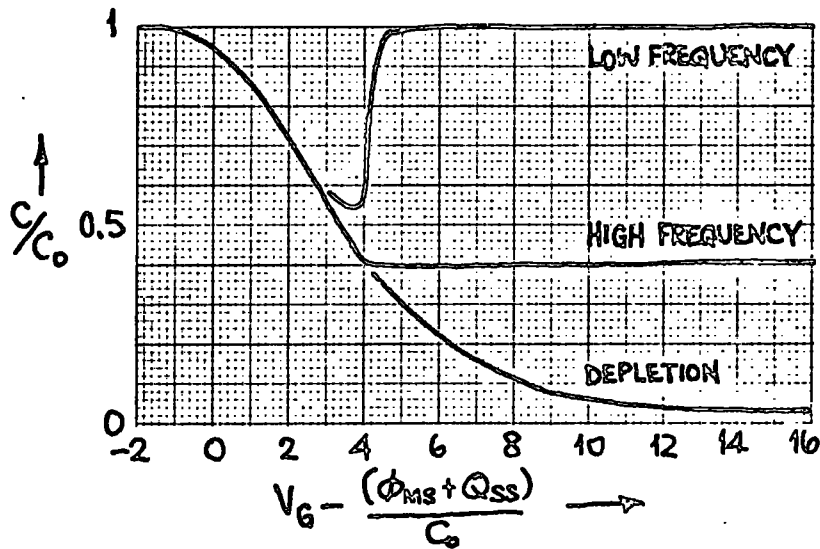
Fig. 5-1: The general form of C-V curves obtained for MOS structures. ϕ_{MS} = metal–semiconductor work–function difference, Q_{ss} = charge in surface states, C_o = oxide capacitance.

Fig. 5-2: (a) The effect on C-V curves of surface states with
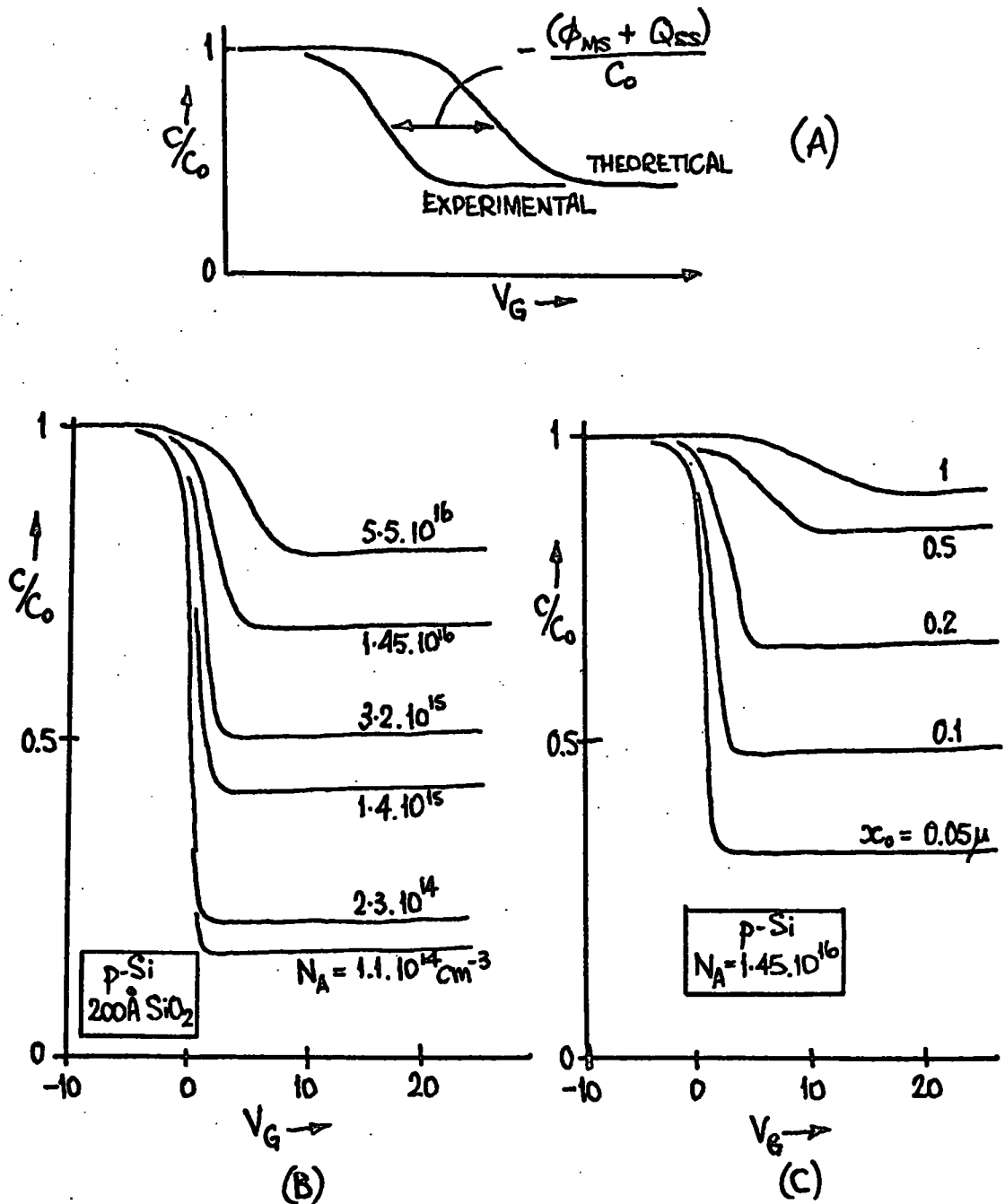positive charge above a p-substrate. ϕ_{MS} = metal-semiconductor
work-function difference, Q_{ss} = charge in surface states, C_o =
oxide capacitance. (b) The effect of doping levels in the silicon.
(c) The effect of oxide thickness. After Grove et al [5].

similar to those in Figs. 5-2(b) and (c).

Snow et al [7] conducted tests on p-channel MOS devices with alkali ions contaminating the outer oxide surface, and from C-V measurements deduced that:

(a) if a steady negative bias is applied to the metal contact while the device is heated, the C-V curves are unchanged;

(b) positive bias during heat treatment causes the ions to accumulate at the semiconductor/oxide interface, and shifts the C-V curve negatively (Fig. 5-3); and

(c) process (b) is reversible by short-circuiting the device, or applying negative bias, during heat treatment.

These techniques are known as bias-temperature (BT) experiments, and are widely used.

Shewchun and Waxman [6] recognised the disadvantages of point-by-point C-V measurements and developed an instrument for automatic plotting of either C-V or G-V characteristics. Their instrument is similar in principle to that described in Sections 5-3 to 5-6: a simplified block diagram is given in Fig. 5-4.

Bias from a motor-driven high voltage sweep generator and an a-c signal of 10-100mV are applied to the device under test, and the a-c current through the device is detected by a current transformer with a low impedance primary winding (30Ω). Signals and noise are amplified, filtered and rectified in a phase-
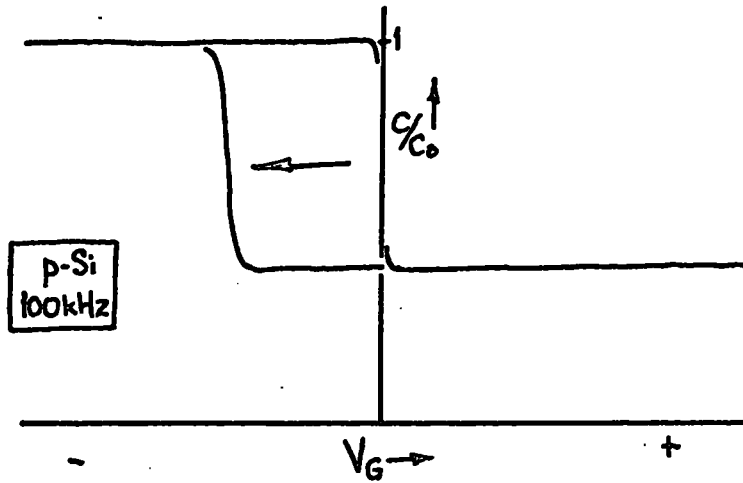
Fig. 5-3: Effect of ion accumulation at the oxide-semiconductor
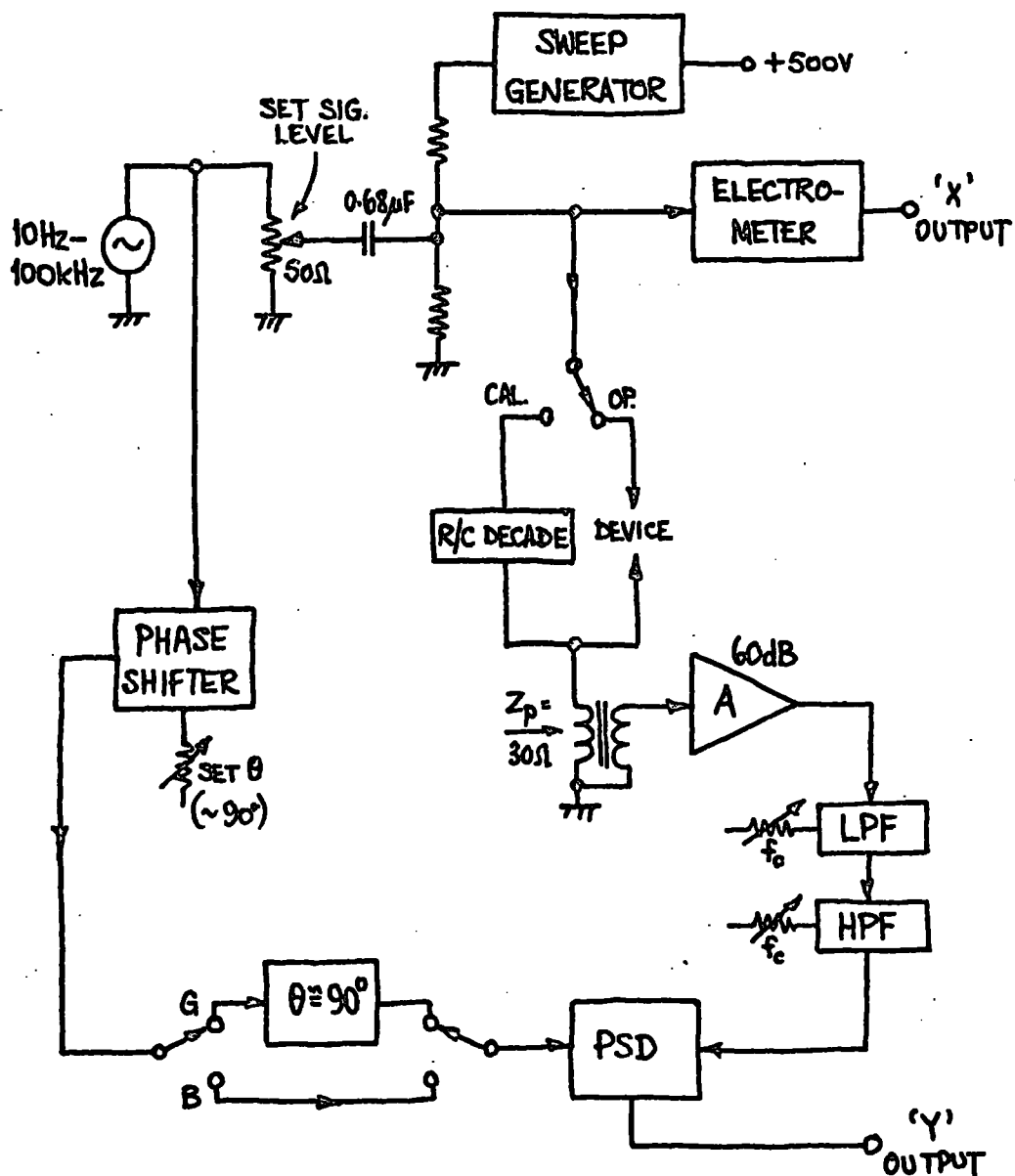interface, with a p-type silicon substrate.

Fig. 5-4: Simplified block diagram of the conductance-capacitance plotter devised by Shewchun and Waxman .

sensitive detector (psd). By shifting the psd reference
signal by 90° or 180°, the detector will reject the resistive
or reactive part of the device current, enabling the other
component to be measured. A calibrator is included to
determine the instrument sensitivity. The specification of the
Plotter described by Shewchun and Waxman was as follows:

Frequency range: 10Hz - 100kHz

Admittance range: 100u℧ - 1n℧ (100dB)

Detection sensitivity: 3.2nV

Maximum $\frac{G}{B}$ ratio: $\pm$80dB

Capacitance range: 16pF - 1.6µF (10Hz)

0.16pF - 16nF (1kHz)

0.0016pF - 160pF (100kHz)

The versatility of the instrument can be improved in
several ways, and in ~~plotting~~ ^{designing} the G-C-V Plotter described later,
the following design aspects were examined:

(a) The ability to measure conductance and capacitance
simultaneously by the use of two psd's.

(b) extending the admittance range down to 100p℧ (10GΩ), and
improving the dynamic range to 140dB.

(c) The ability to measure capacitance between 1 and 1000pF
over the whole frequency range.

(d) The use of a switchable current-sensing resistor in place

of the original transformer to provide variable detection sensitivity.

Danby has published several designs for advanced phase-sensitive detectors: in particular his double-balanced psd (Fig. 5-5) overcomes some of the disadvantages of the well-known long-tailed pair circuit (Fig. 5-6). The double-balanced circuit has (see Appendix A):

(a)   a single-ended rather than differential output, which offers a saving in averaging capacitors and convenience when used with an external recorder;

(b)   balance conditions which depend on the matching of psd components and which are independent of the mark-space ratio of the reference square wave; and

(c)   slightly lower intermodulation distortion, due to its double-balanced topography.

On the other hand, the double-balanced circuit is considerably more complicated.   When considering point (b) it was decided it would be preferable to treat the problem at its source, rather than rely on the matching of transistors and other components. A long-tailed pair psd was therefore designed, with the reference signal provided by a specially developed precision squaring circuit.

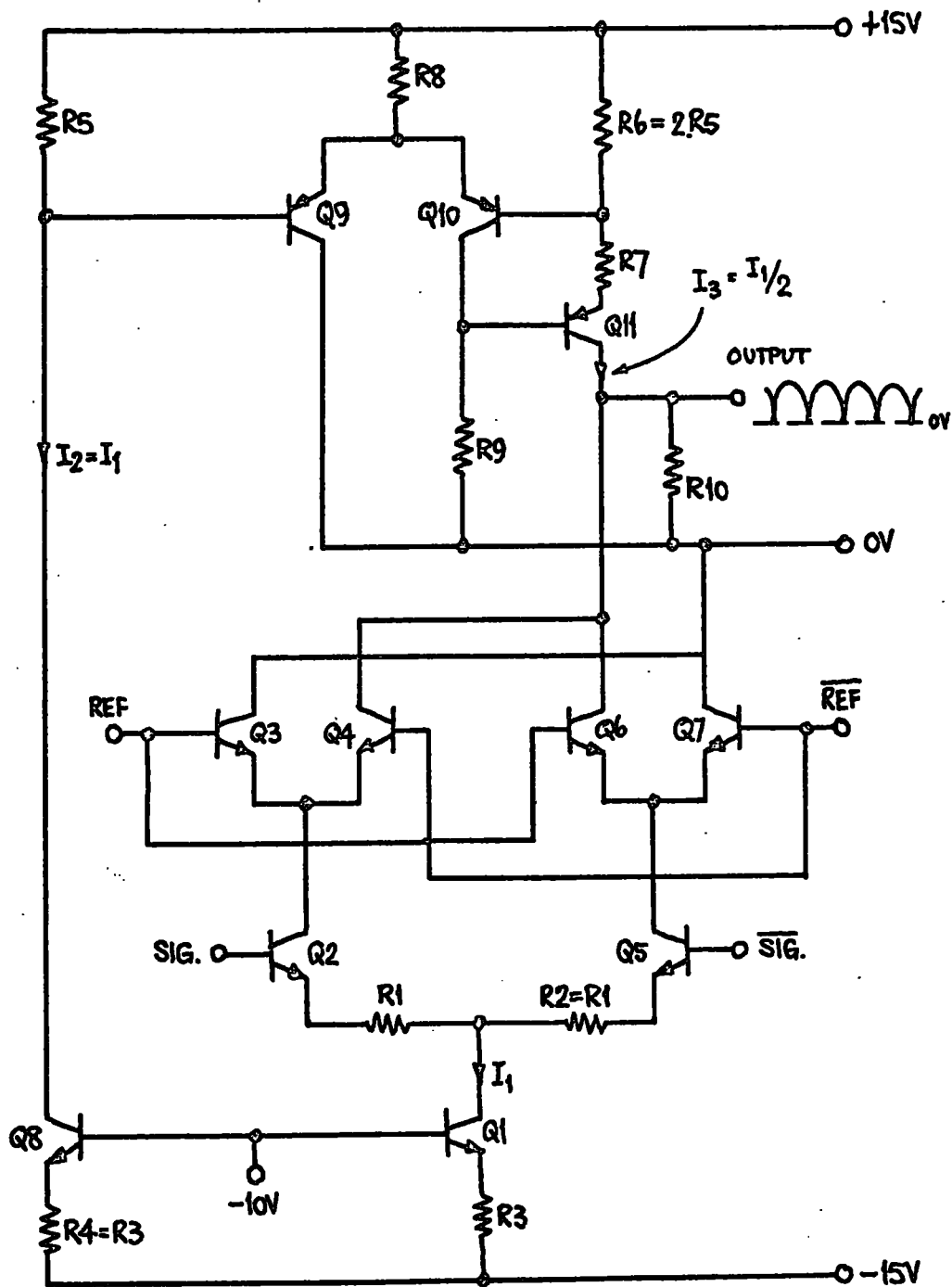Fig. 5-6 shows the long-tailed pair psd with input and output

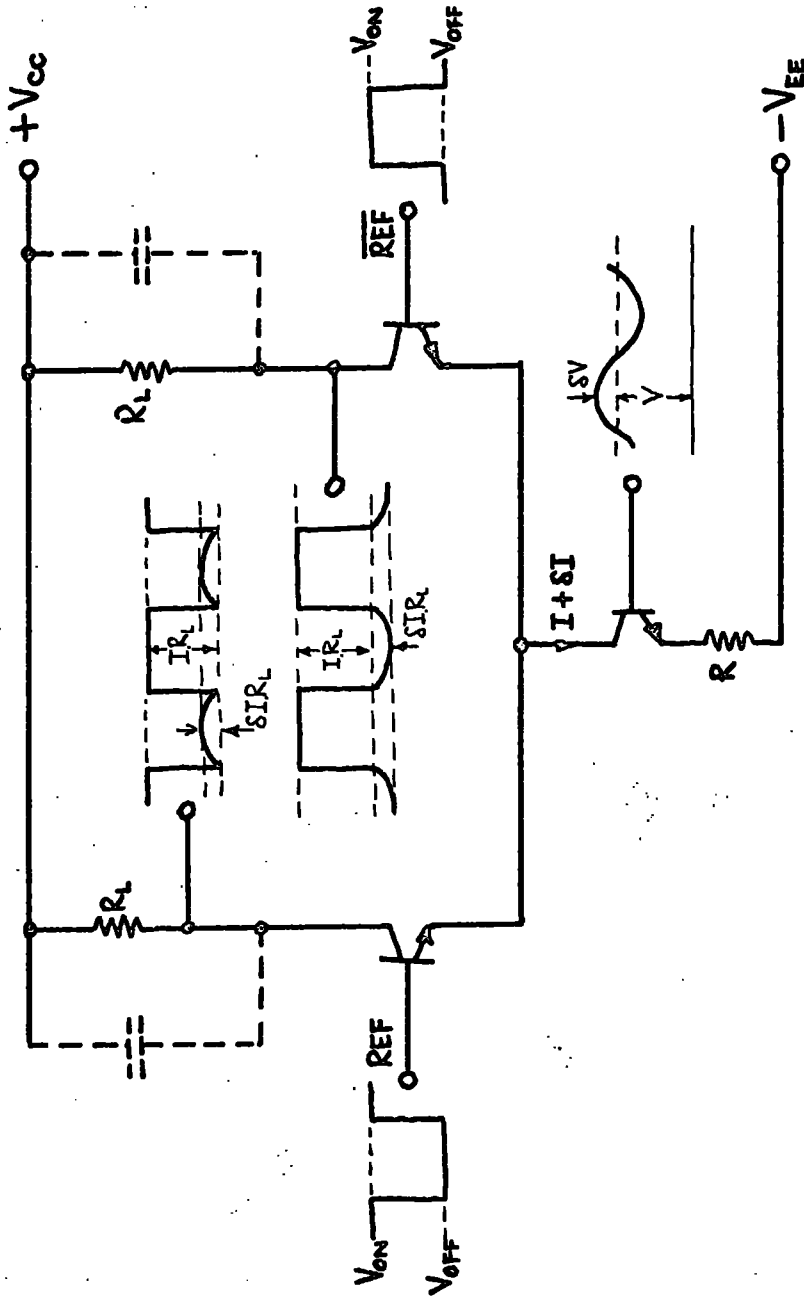Fig. 5-5: The double-balanced phase-sensitive detector, after Danby [8].

Fig. 5-6: The long-tailed pair phase-sensitive detector.

waveforms for an in-phase signal. The unsmoothed output waveforms consist of a half-wave rectified sine wave super-imposed on a square wave of amplitude $I.R_L$. On smoothing, the differential output is the difference of the two average values of the two half-sine waves. The average value of a full-wave rectified sine wave, amplitude $\delta I.R_L$, is:

$$\frac{1}{\pi}\int_0^{\pi} \delta I.R_L. \sin \theta. \, d\theta \quad = \quad \frac{2\delta I.R_L}{\pi} \qquad \dots \text{(5-1)}$$

and $$\delta I = \frac{\delta V}{R}$$

where δV is the peak value of the input signal, and R is the tail transistor emitter resistance. The voltage gain (A_V) of the psd is therefore:

$$A_V = \frac{V_O}{V} = \frac{2R_L}{\pi R} . \qquad \dots \text{(5-2)}$$

In the circuit developed, $R_L = 3.3k\Omega$ and $R = 1.5k\Omega$. Thus $A_V = 1.40$.

6-3 Instrument specification

Much of the interest in G-V and C-V measurements is due to the frequency-dependent effects observed, and judging from previous work, especially on MOS structures, the frequency range of interest extends from 10Hz to about 100kHz. The present G-C-V Plotter was therefore designed to operate accurately over this

range, and up to 800kHz with some loss of accuracy.

It was decided that the Plotter should be designed to measure capacitance in the range 1-1000pF. Few devices exhibit capacitances below 1pF, and a range extending to about 1000pF will accommodate most MIS display devices. With measurement frequency varying over five decades, it is apparent that the capacitive reactance of devices will vary over seven or eight decades. 1pF at 10Hz has a reactance of 16GΩ, whereas 1000pF at 100kHz has 1600Ω. This corresponds to a dynamic range of 140dB. At all stages of instrument design, steps have therefore been taken to cover as much of this range as possible.

The circuits involved in the measurement of conductance and capacitance are identical, and have the same dynamic range. In spite of the fact that some parts of the instrument are common to both channels, it is possible to measure very high susceptance and low conductance simultaneously, and vice versa. This is an important design feature.

A mid-range target figure for instrument accuracy of one or two per cent was adopted. The Plotter was provided with an external calibrator having switched capacitance (2-1000pF ±1%) and conductance (0·01μ℧ ±10% and 0.03-100μ℧ ±0.1%).

Visual output is provided by two 3½-inch meters showing conductance and capacitance. A recorder output is available from each channel and from the sweep voltage generator, for operating

an X-Y recorder.

An external oscillator provides the signal voltage applied to the device under test and to the reference circuits in the instrument. This signal should be 100mV (nominal) for correct operation, but a front-panel potentiometer is provided to reduce the signal voltage reaching the device. To reduce output jitter, it is important that the external oscillator has high phase stability. Some commercial laboratory oscillators (e.g. Venner TSA 625, Advance H-1) were found to be inadequate in this respect and were rejected in favour of an FET Wien Bridge laboratory oscillator developed and built in the Department.

The block diagram of the complete G-C-V Plotter, as designed, is shown in Fig. 5-7, although some switching is omitted for clarity.

The a-c and sweep voltages are applied to the device under test, and the complex a-c current due to its admittance $(Y = G + jB)$ is detected by a current-sensing resistor R. The small signal voltage developed across this is processed in a low-noise high gain amplifier, and low-pass and high-pass filters, before reaching the two phase-sensitive detectors. These isolate the resistive and reactive components of the original device current, and provide two d-c output signals for measurement.

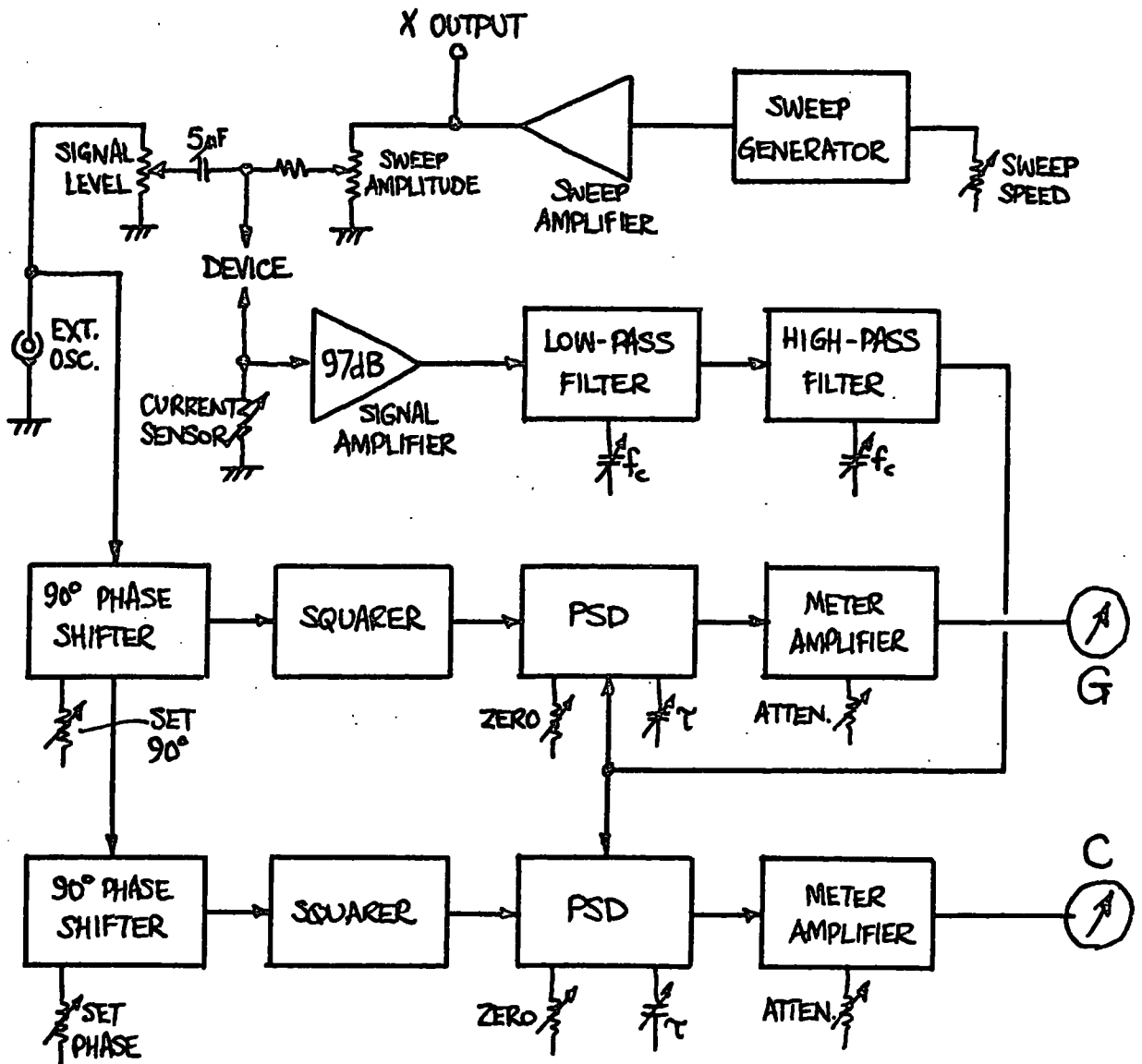The psd's are of the type which give zero output when the

Fig. 5-7: Block diagram of the G-C-V Plotter.

signal and reference voltages are 90° out of phase. The a-c

signal from the external oscillator is therefore phase-shifted

twice through 90° (neglecting any spurious phase-errors which

must be corrected for) to provide a suitable reference for each

psd. These reference signals are accurately squared in a novel

feedback circuit (see Section 5-5).

Various accessory circuits have been designed for use in

the instrument. The stabilised four-rail power supply and an

overload indicating circuit are examples.

5-4 The signal amplifiers

The design requirements for the main signal amplifier are

stringent. To achieve one per cent accuracy, the a-c voltage

developed across the current-sensing resistor must be less than

one per cent of the applied signal voltage. This would be 100μV

for 10mV applied, but this applies to the larger of the two current

components, resistive or reactive. As it is desirable to measure

one component up to 10,000 times the other, the minimum signal

the instrument must resolve is of the order of 10 nV. A signal

amplifier gain of 100dB is sufficient for such signals to operate

the psd's satisfactorily.

The main problems associated with the design of the

signal amplifier are (a) noise, and (b) achieving sufficient gain,

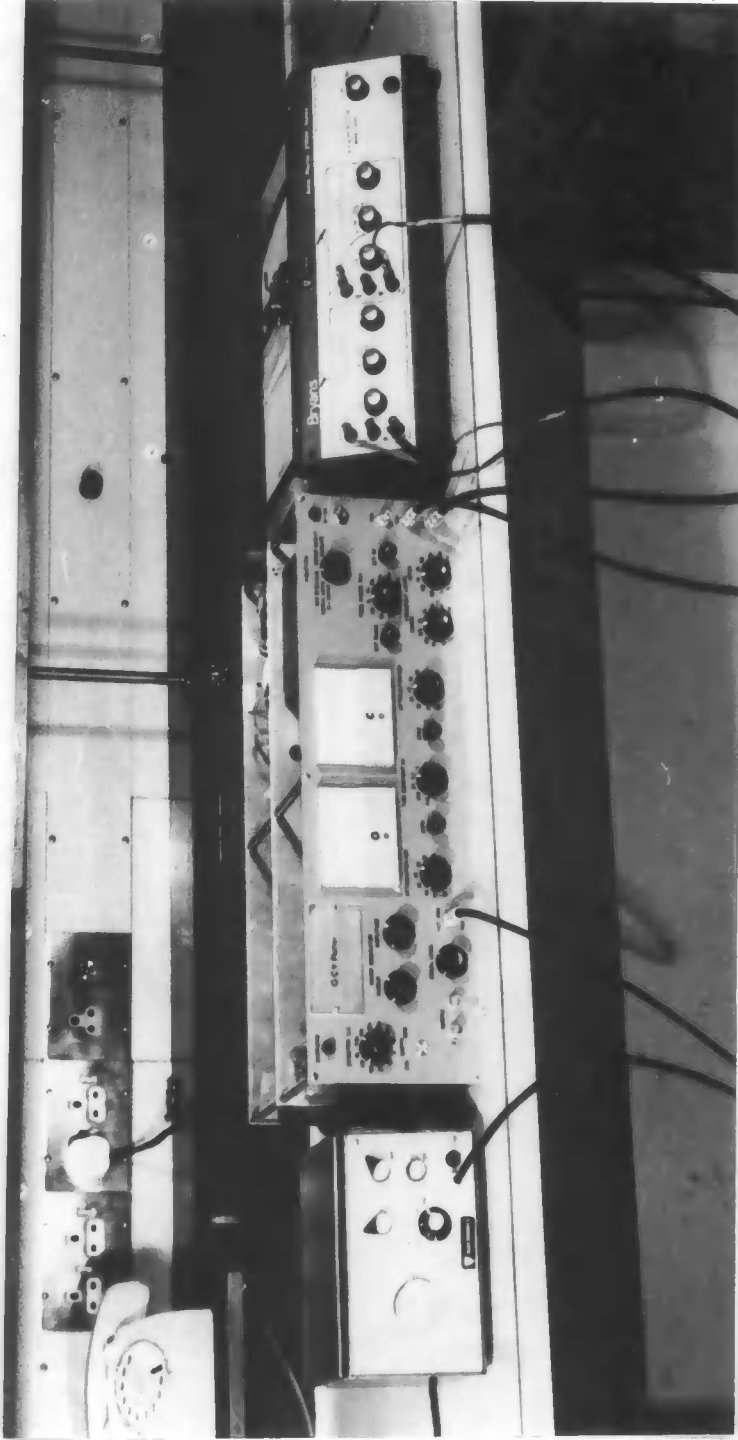bandwidth and freedom from spurious phase-shifts. The circuit

Plate 5-1: The G-C-V Plotter in use with a Bryans X-Y recorder and a Department-designed Wien Bridge oscillator.

developed has a low-noise JFET preamplifier (Texas 2N3822: Q1 in Fig. 5-8) followed by a high gain d-c coupled pair (Q2, Q3) and a high-frequency compensation stage (Q4). C1 is selected for optimum amplifier square-wave response. An emitter follower (Fig. 5-9), external to the screened main amplifier, provides a low output impedance for a coaxial interconnecting cable. The overall gain is 97dB (see Fig. 5-9), and the 3dB bandwidth is 10Hz to 800kHz. The amplifier phase-shift is 60° at 10Hz, but only 15° at 300kHz.

The Texas 2N3822 FET was chosen for Q1 because of its good low-frequency noise figure (less than 5dB at 10Hz for a 1M generator resistance), and high mutual conductance $(3-6\cdot 5\text{m}\mho)$. The generator resistance to give minimum noise figure depends on the measurement frequency: at high frequencies a lower resistance is preferable. In the Plotter the generator resistance is the current-sensing resistor R: at low frequencies this tends to be high (up to $1\text{M}\Omega$) because of the high capacitive reactances encountered. At high frequencies R tends to be low (down to 10Ω). Because of this the preamplifier runs near the optimum conditions at all operating frequencies.

Several good low-noise p-channel JFET's are available, but these have higher input and feedback capacities, so that n-channel devices such as the 2N3822 are preferable.

The bandpass amplifier (Fig. 5-10) is used to limit the
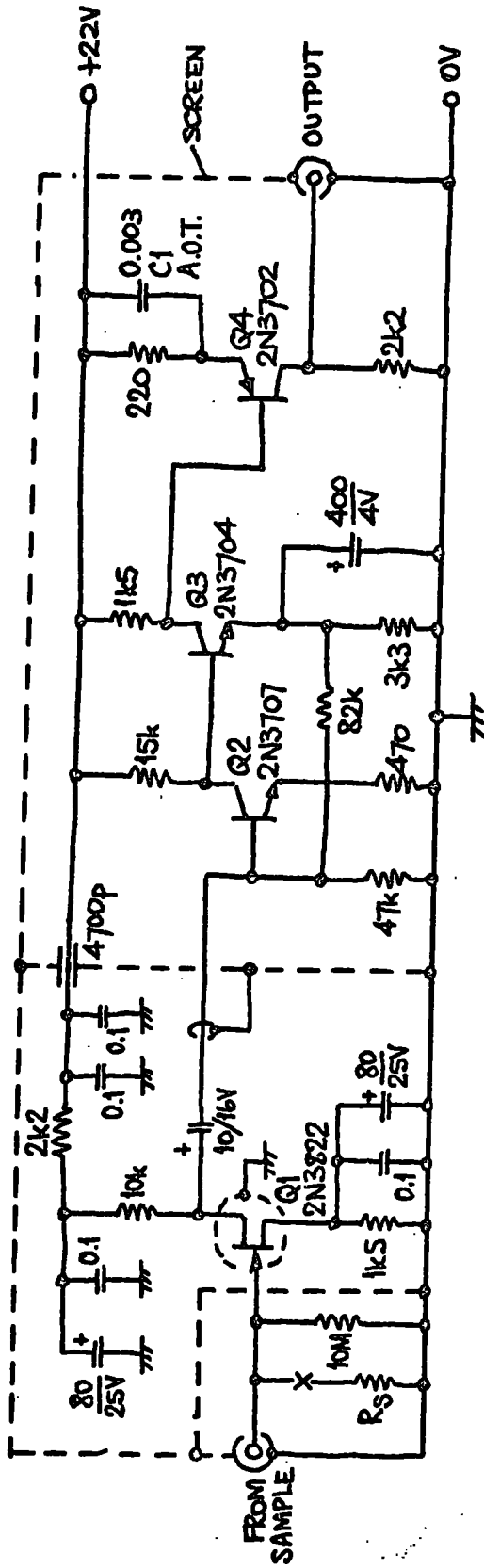
RESISTANCE IN OHMS, CAPACITANCE IN MICROFARADS, UNLESS OTHERWISE STATED.
R_S IS SWITCHABLE TO 0, $\frac{1}{10}$, $\frac{1}{3}$0, 100, 300, 1k, 3k3, 10k, 33k, 100k, 330k, or 1MΩ.

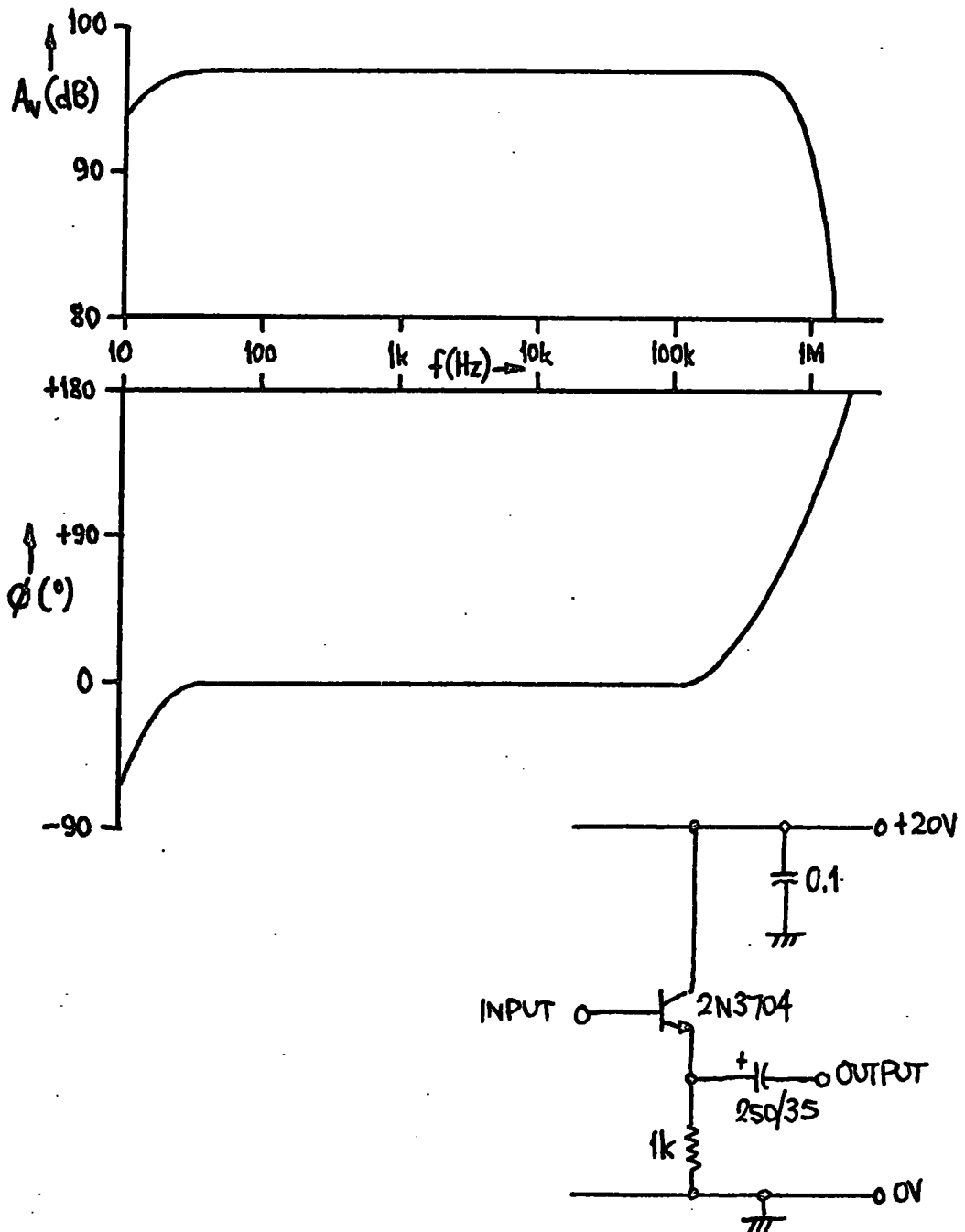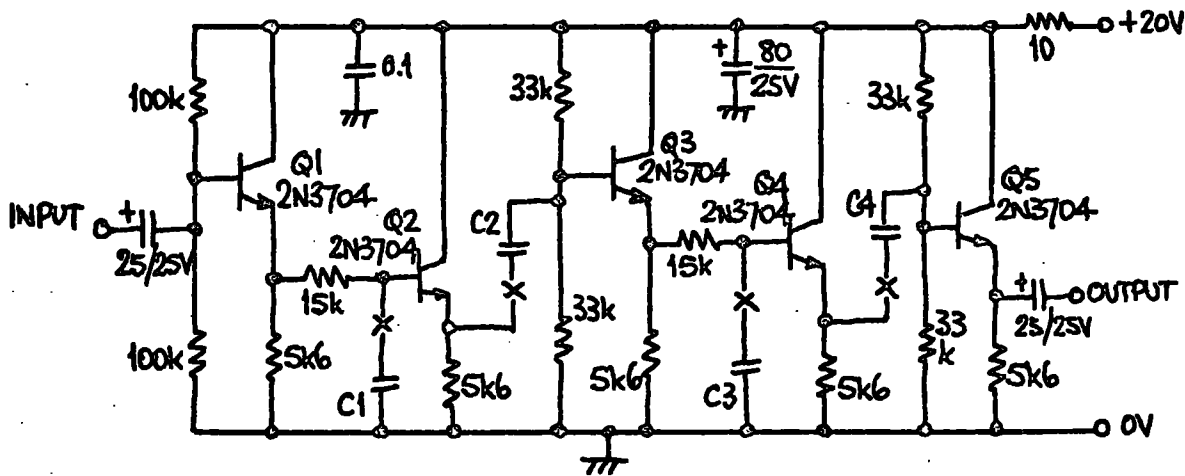Fig. 5-8: The low-noise signal amplifier.

Fig. 5-9: <u>Top</u>: Frequency and phase response of the C-C-V
Plotter signal amplifier. <u>Bottom</u>: Emitter follower used to
match the signal amplifier to a coaxial line.

RESISTANCE IN OHMS, CAPACITANCE IN μF, UNLESS OTHERWISE STATED.

Fig. 5-10: The C-C-V Plotter bandpass amplifier, used to reduce system noise bandwidth.

signal channel bandwidth in order to reduce noise. Low
frequency noise in particular is troublesome if it reaches the
X-Y recorder.

The bandpass amplifier has upper and lower cut-off
frequencies switchable in 1-3-10 sequence over the entire
frequency range of the instrument. A slope of 40dB per decade
in the stopbands is achieved by cascaded low-pass and high-pass
R-C sections, isolated by emitter followers. The low-pass
sections are based on source resistances of 15kΩ and capacitors
C1 and C3 (see Table 5-1). The high-pass sections have load
resistances of 15kΩ and capacitors C2 and C4. The five emitter
followers are biased to give the maximum possible output voltage
swing ($\pm$9V), in order to preserve the dynamic range of the
instrument.

f_c (Hz)	3	10	30	100	300	1k	3k	10k	30k	100k	300k
C1, C3 (F)	3µ	1µ	0.3µ	0.1µ	30n	10n	3n	1n	300p	100p	-
C2, C4 (F)	-	1µ	0.3µ	0.1µ	30n	10n	3n	1n	300p	100p	30p

Table 5-1: Bandpass amplifier filter capacitor values.

5-5 The phase-sensitive detectors

The two phase-sensitive detectors are based on a long-tailed
pair (Q1A and Q1B in Fig. 5-11) with a tail transistor (Q2).
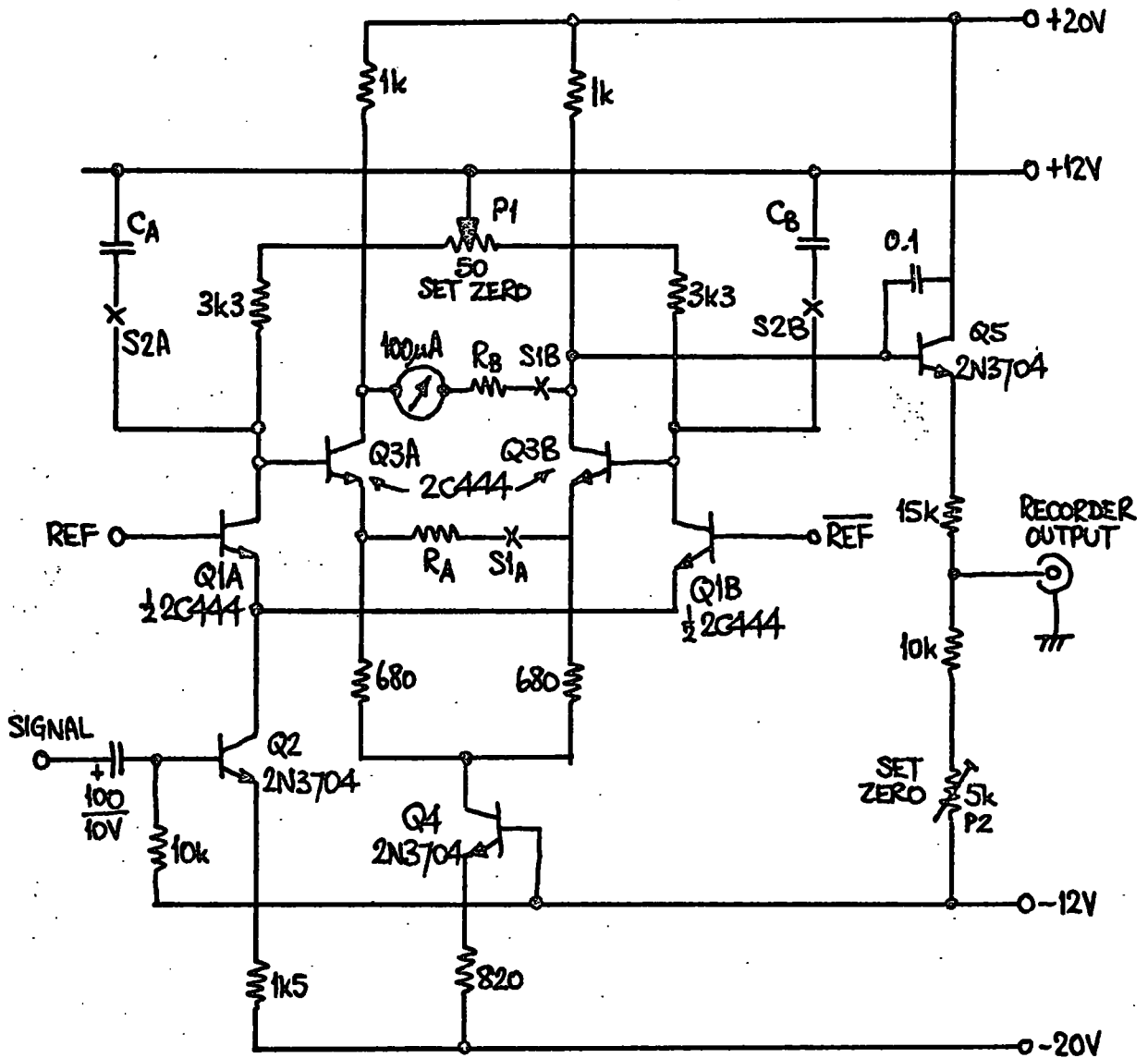
Fig. 5-11: The G-C-V Plotter phase-sensitive detector and meter amplifier. One of these circuits is needed for each channel of the instrument. Psd time constant is switchable from 0.01 to 3 seconds.

Signal input, with noise, is applied to the base of Q2, and the complementary squared reference signals switch the differential pair. The psd output is averaged with a time constant determined by C_A, C_B and the $3 \cdot 3 k\Omega$ load resistors, and is fed to the variable-gain differential meter amplifier (Q3A, Q3B). Q5 is an emitter follower providing a single-ended recorder output.

The d-c voltages at various points in the psd's and meter amplifiers have been chosen for high dynamic range. The ON transistor in the psd (Q1A or Q1B) has zero base voltage, so the input signal at the base of Q2 can swing 11V positive and 8V negative. With no input signal the collectors of Q1A and Q1B are at +14V: the maximum differential psd output is therefore $\pm$8V. A 50Ω potentiometer (P1) in the collector circuit of Q1 balances the psd and meter amplifier against spurious d-c offset voltages in the circuit. These are minimised by the use of matched thermally-coupled transistors in a single can (SGS 2C444) for Q1 and Q3.

The meter amplifier is a long-tailed pair with emitter coupling switchable to vary the gain (R_A, S1A). By also switching the 100μA meter multiplier resistor (R_B, S1B) in the collector circuit of Q3, up to 60dB of gain variation is realisable. S1A and S1B are ganged, and form the ATTENUATION control, calibrated from 0 to 60dB in steps of 10dB. Table 5-2 shows the values of R_A and R_B used.

Attenuation (dB)		0	10	20	30	40	50	60
R_A	(Ω)	0	0	0	0	130	770	∞
R_B	(Ω)	0	5060	21k	71.6k			$\longrightarrow$

Table 5-2: Values of R_A and R_B associated with the meter amplifier (Fig. 5-11).

Under no-signal conditions the collector voltage of Q3A and Q3B is about +15V. The emitter circuit of the recorder output amplifier Q5 reduces this to zero, simultaneously attenuating the single-ended meter amplifier output by a factor of about two. P2 is a preset potentiometer used to set the zero at the recorder output of each channel.

As discussed in Section 5-2, the balance of the psd's used is dependent on the mark-space ratio of the reference square-waves. In view of the instrument accuracy required, it was important to develop circuits which would accept sine waves over a wide range of frequencies and amplitudes, and produce square-waves with unity mark-space ratio within very fine limits. Fig. 5-12 shows the circuit devised.

The circuit is based on a Schmitt trigger circuit (Q3, Q4) with its input biasing controlled by a feedback loop. The output of the Schmitt trigger circuit at the collector of Q4, and the inverted output at the collector of Q5, are averaged by R1-C1 and R2-C2 and compared in the differential amplifier Q6, Q7.
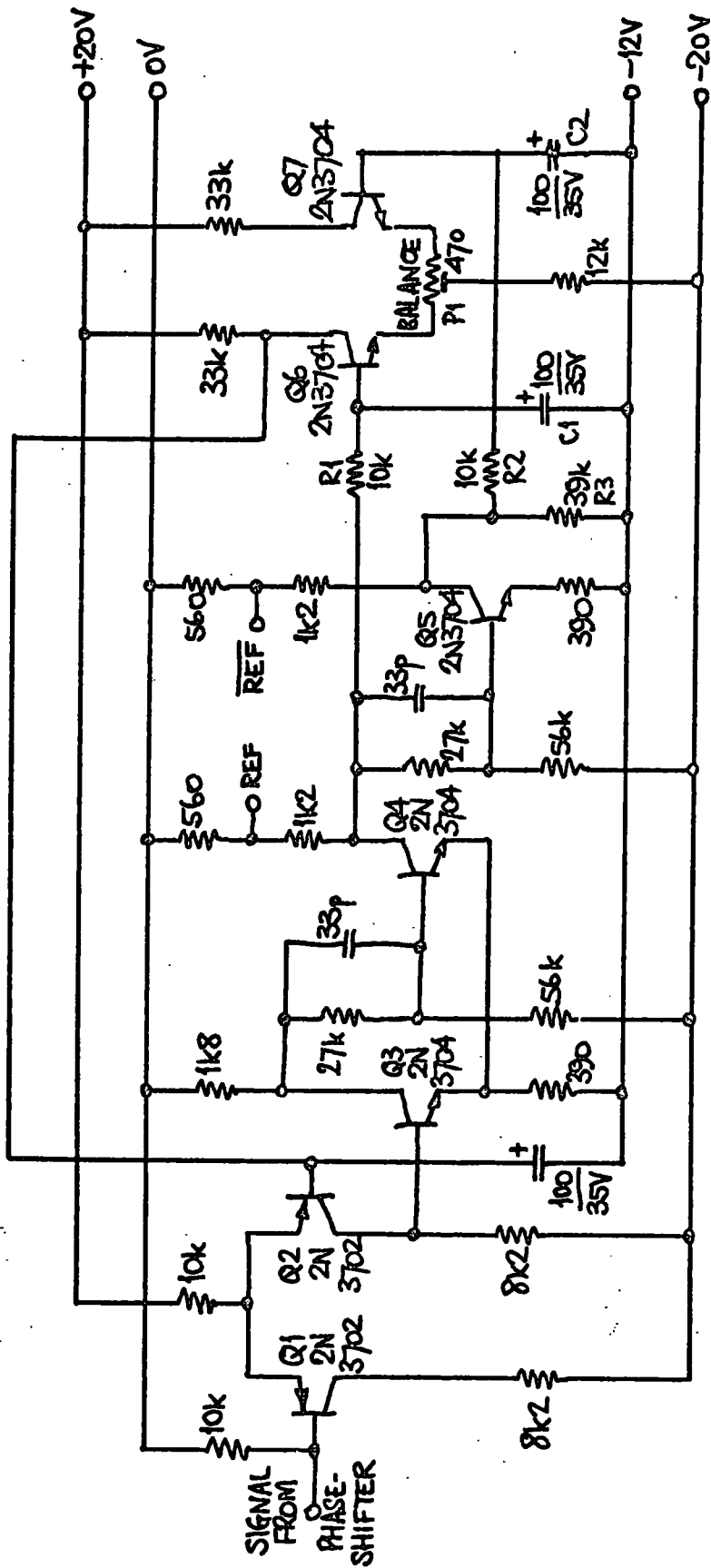
RESISTANCE IN OHMS, CAPACITANCE IN MICROFARADS, UNLESS OTHERWISE STATED.

Fig. 5-12: The precision squaring circuit.

The output of this is further smoothed and used to bias the Schmitt trigger circuit via the input differential pair Q1, Q2. The input reference sine wave is superimposed on the bias voltage, again via Q1, Q2.

If the mark-space ratio of the reference square-wave is exactly unity, Q6 and Q7 will be balanced and the Schmitt trigger will be biased at a suitable operating point. Any change in mark-space ratio will unbalance Q6 and Q7, and shift the bias point to cancel the change. The BALANCE potentiometer P1 is used to set the mark-space ratio to unity.

Correct operation of the circuit depends on the voltage levels at the collectors of Q4 and Q5 being equal and well-defined. R3 is connected between the collector of Q5 and -12V to cancel the effect caused by R4 and R5 loading the collector of Q4. Speed-up capacitors are used in the Schmitt trigger and the inverter to obtain the fastest possible rise-time (70ns).

Good frequency independence of the mark-space ratio of the output square-waves REF and $\overline{\text{REF}}$ is inherent in the nature of the circuit. Independence of the amplitude of the input sine wave is partly due to symmetrical clipping in the input differential pair Q1, Q2. Table 5-3 summarises the errors caused by changes in sine wave frequency and amplitude, and by changes in the supply voltages.

V_{in} (pk-pk)	0.05	0.1	0.2	0.5	1.0	2.0	5.0	
Error (%)	-0.20	-0.20	-0.12	-0.02	0.0	+0.02	+0.04	

f (Hz)	10	30	100	300	1k	3k	10k	30k	100k
Error (%)	+0.10	+0.47	-0.02	-0.10	-0.04	-0.07	+0.02	+0.03	0.0

Supply voltage dependence: less than 0.1% error for ±10% change in any supply voltage.

Table 5-3: Errors measured in squarer mark-space ratio.

The measurement of the mark-space ratio of the reference square-wave to an accuracy of 0.02% or better presented a problem, as the use of a digital timer/counter would involve making up some additional circuits. The procedure adopted involved the delay timebase of a Tektronix 545 oscilloscope. This has an accurately calibrated ten-turn potentiometer to set delay time, and this can be used to measure the mark-time and space-time in arbitrary but identical units.

When using the G-C-V Plotter, and small errors in mark-space ratio brought about by changes in operating frequency can be offset by the ZERO potentiometer associated with each psd. Errors due to changes in signal amplitude rarely occur, as the Wien Bridge oscillators normally used with the instrument have excellent output voltage regulation.

The sine-wave reference signal for each squaring circuit is derived from the dual phase-shifting circuit (see Fig. 5-13). The entire six-stage circuit, consisting mainly of emitter followers and split-load phase-splitters, is d-c coupled. The phase shift in Q3 or Q5 at any frequency depends on the product R-C, where C is switched to cover the frequency range 3Hz to 300kHz. Potentiometers R are front-panel controls with epicyclic slow-motion drives used to set the phase shift in each stage.

The signal reaching the base of Q4 is predominantly from the collector of Q3 if R is zero, and the stage phase-shift is 180° (neglecting the output impedance at the collector of Q3). If R is infinite, the output signal is from the emitter of Q3 and the phase-shift is zero. If R is equal to the reactance of C at the operating frequency, then the phase-shift is 90°. The collector output impedance of Q3 or Q5 is about 1kΩ, and R has a maximum value of 10kΩ, so the frequency range over which a signal phase-shift of 90° can be obtained is about 11:1. Some overlap of frequency ranges is provided by switching the capacitors C in a 1-3-10 sequence.

It is important that the phase-shifts introduced by these circuits are stable with time. For this reason electrolytic capacitors have not been used for the low-frequency values of C, in preference for polyester types.

The phase-shifter setting-up procedure is described in
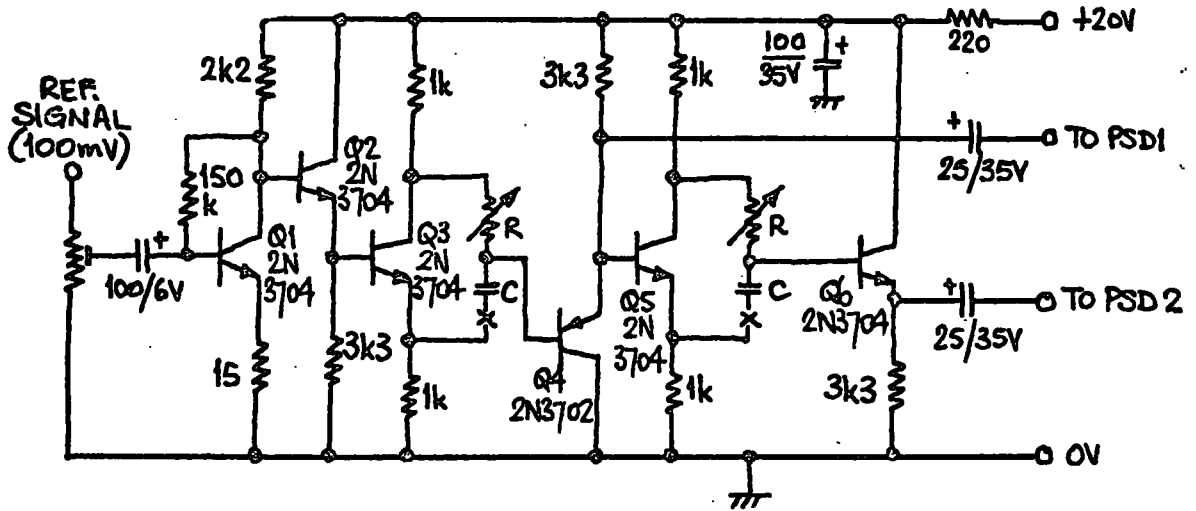
ALL RESISTANCES IN OHMS, CAPACITANCE IN μF, UNLESS OTHERWISE STATED.

Fig. 5-13: The G-C-V Plotter dual phase-shifter.

Section 5-7.

5-6 <u>The sweep generator and power supplies</u>

The sweep generator is almost identical to that developed for the C-V Plotter (Chapter 4). The circuit (Fig. 5-14) is again based on an integrator controlled by a Schmitt trigger circuit. Q1 has been added in place of the two diodes to provide a greater range of d-c shift for the integrator output voltage.

Because of the time constants associated with the psd collector circuits, lower sweep speeds are needed. The range of sweep periods provided by the SWEEP SPEED potentiometer is from 20 seconds to 15 minutes. The integrator circuit was found to function satisfactorily with sweep periods of up to 40 minutes.

The four-rail power supply for the G-C-V Plotter is shown in Fig. 5-15. The four stabilisation circuits are similar and based on series regulator transistors (Q3, Q7, Q11, Q15). Considering the +20V supply, Q2 compares the voltage divider output at the slider of P1 with the 9·1V reference, and controls the base of Q3. Q1, with the 4·7V Zener diode, forms a constant current source to reduce ripple on the output. Q4 provides short-circuit protection by clamping the base of Q3 when the load current exceeds about 100mA. Because of the high current demand from the +20V supply, Q3 is a heat-sinked BFY17 transistor. Q7, Q11 and Q15 are epoxy types (n-p-n 2N3704 or p-n-p 2N3702).
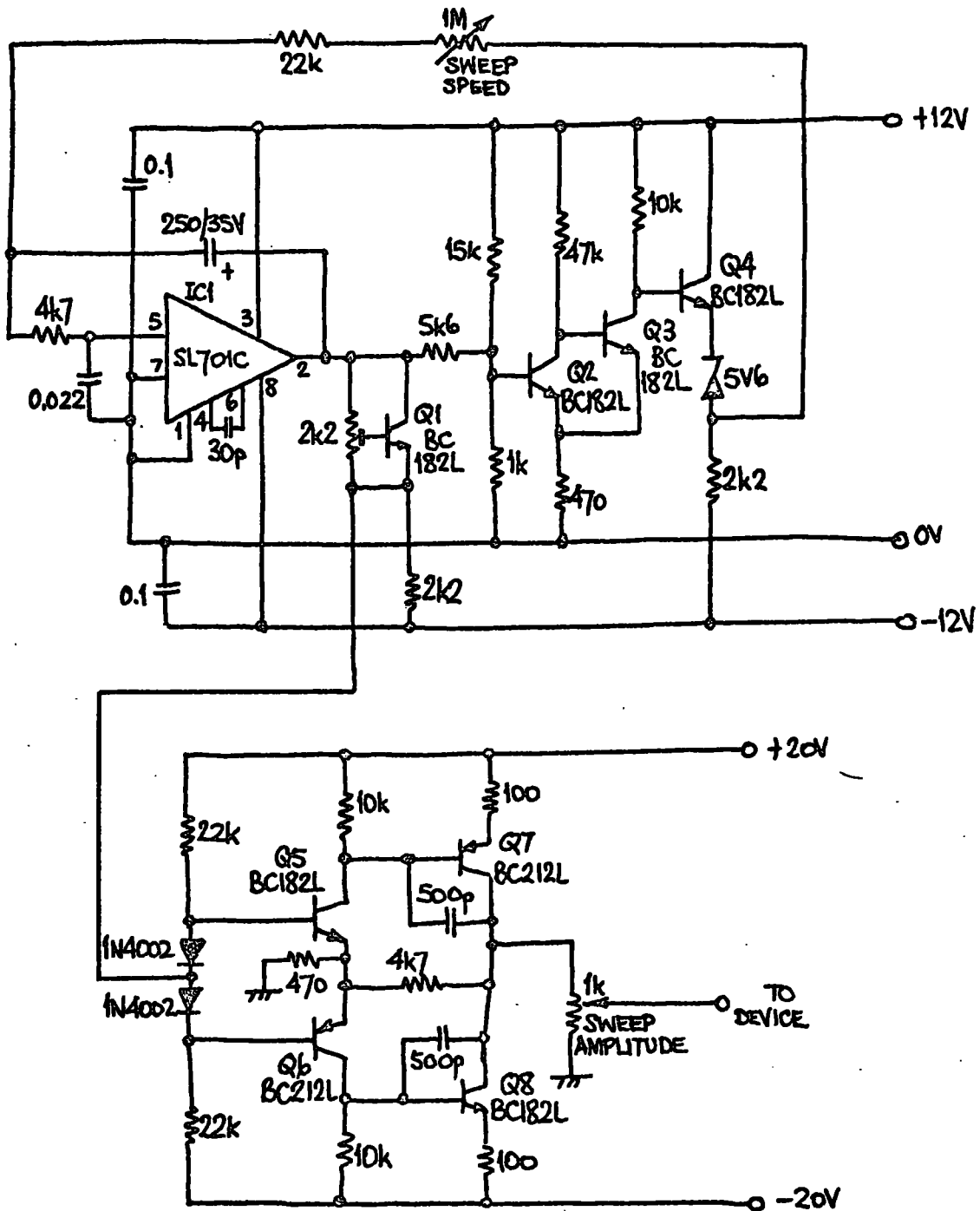
RESISTANCE IN OHMS, CAPACITANCE IN µF, UNLESS OTHERWISE STATED.

Fig. 5-14:   The G-C-V Plotter sweep generator and amplifier.
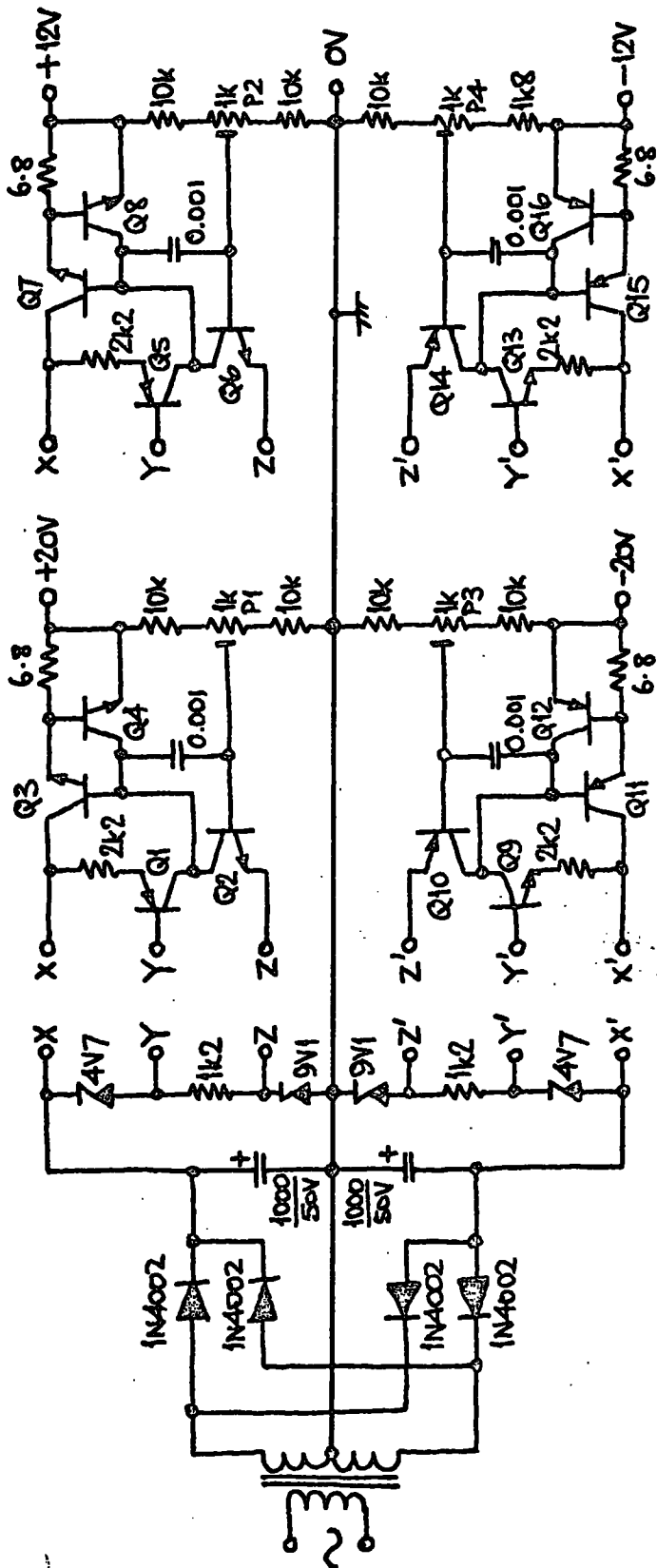
RESISTANCE IN OHMS, CAPACITANCE IN μF, UNLESS OTHERWISE STATED. ALL NPN TRANSISTORS
2N3704 (EXCEPT Q3: BFY17); ALL PNP TRANSISTORS 2N3702.

Fig. 5-15: The four-rail G-C-V Plotter stabilised power supply.

The performance of the four regulated supplies is summarised below:

D-c load regulation: 3mV change in output for a 50mA
                       change in load current.

Output ripple: Less than 1mV rms.

Load transient recovery time: 400ns.

Interaction between supplies: Less than 500μV change
                       in output from one supply for a 50mA
                       change in load current from any
                       other supply.

All supply leads to signal-handling stages of the instrument are screened to reduce interaction between circuits. In particular the high gain signal amplifier is susceptible to transients on supply rails created by the switching transistors in the squaring circuits. The squaring circuits and phase-sensitive detectors are fully screened, as are the main signal amplifier and the phase-shifter.

Due to the extremely low signal levels involved and the complexity of the instrument, it was anticipated that earth loops might introduce spurious signals which would limit the dynamic range of the Plotter. During tests it was found that earth loops associated with the calibrator switches affected their usefulness, and for this reason an external calibrator has been

built (Fig. 5-16). Apart from this it was only necessary to connect two earth straps between units to reduce circulating currents to an undetectable level. The detection sensitivity of the instrument was measured as 10nV for a 10dB signal-to-noise ratio.

5-7 Operating procedure

The G-C-V Plotter is set up initially as follows:

(a) Connect the external oscillator (100mV rms output), set the SIGNAL LEVEL potentiometer to maximum, and switch the phase-shifter FREQUENCY RANGE to the appropriate position. Select a suitable DETECTOR resistor, based initially on the expression $R = 10^6/f$, where f is in Hz. Turn the SWEEP PERIOD and AMPLITUDE controls fully anticlockwise.

(b) Set the TIME CONSTANT to one second and the ATTENUATION switches to 30dB, and ZERO the two meters.

(c) With 60dB of G ATTENUATION and 40dB of C ATTENUATION, introduce sufficient conductance from the calibrator to deflect the G meter to about half-scale. Zero the C meter by means of the SET 90° potentiometer. Repeat this procedure with 40dB of G ATTENUATION and 60dB of C ATTENUATION, and a capacitance from the calibrator, using the SET PHASE control. Finally set both ATTENUATION controls to 60dB.
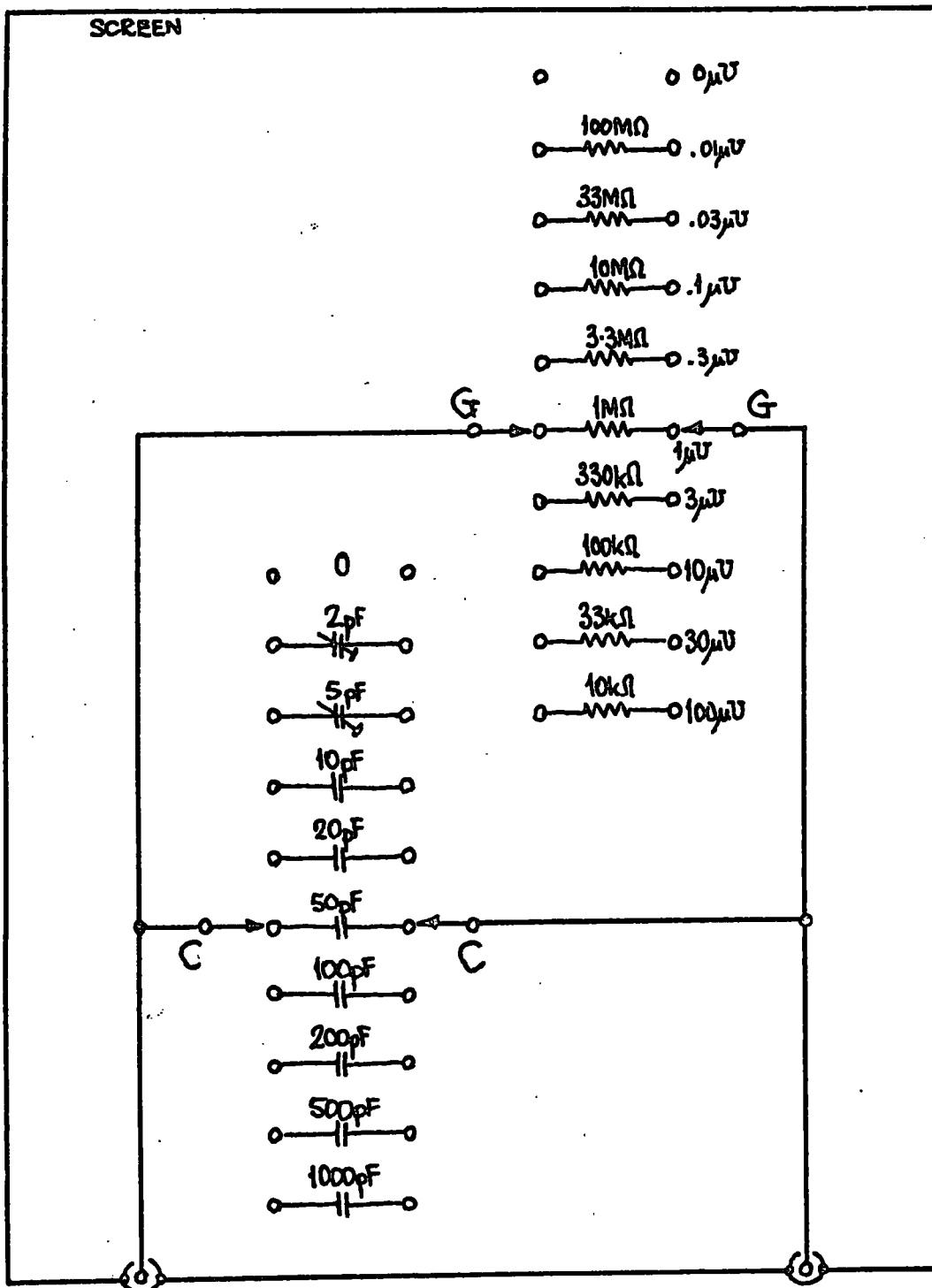
80.

Fig. 5-16: Calibrator built for use with the G-C-V Plotter.

The instrument is now ready for use. A preliminary study of the behaviour of a device may be undertaken as follows:

(a) Plug in the device, set the SWEEP SPEED to a suitable position, and observe the two meter readings. Higher sensitivity can be obtained from either channel by reducing the ATTENUATION: lower sensitivity by reducing the SIGNAL LEVEL or the DETECTOR resistance. If the DETECTOR resistance is changed, it may be necessary to make slight adjustments to the SET 90° and SET PHASE controls, as described above.

(b) At medium or high operating frequencies the instrument response time can be reduced by decreasing the TIME CONSTANT of the phase-sensitive detectors. Higher sweep speeds can then be used.

A plot of the G-V and C-V characteristics of a device can now be made on the X-Y recorder. After each graph is drawn, the calibrator should be used to establish scaling factors.

5-8 Results

The performance of the instrument has been assessed in some detail. Data for individual circuits inside the Plotter have already been given, but the following figures describe the performance of the complete instrument as a measuring device:

Frequency range:	10Hz – 500kHz
Admittance range:	1m℧ – 100p℧
Impedance range:	1kΩ – 10GΩ
Dynamic range:	140dB
Capacitance range:	1pF – 10μF (10Hz)
	0.01pF – 100nF (1kHz)
	0.0001pF – 1nF (100kHz)
Calibrator stray C:	0.08pF
Calibrator stray G:	Less then 100p℧.
Accuracy:	Approx. 1% fsd + 0.5%

To illustrate the use of the G-C-V Plotter, Fig. 5-17 shows
a conductance-capacitance plot obtained from a Plessey p-channel
MOS transistor. A rapid change in capacitance occurs at a bias
voltage of 4·2V. The shift of this transition point away from
zero bias is due to the work function difference (ϕ_{MS}) between
the aluminium top contact and the semiconductor, and to space
charge effects in the oxide layer. Bias-temperature (BT)
experiments carried out on the same device (+10V applied to
the gate at about 150°C) showed no further negative shift of the
C-V curve due to the movement of impurity ions from the silicon/
silicon dioxide interface to the metal. The absence of impurity
ions is to be expected with good commercial MOS devices.
The peak in the conductance characteristic is due to surface
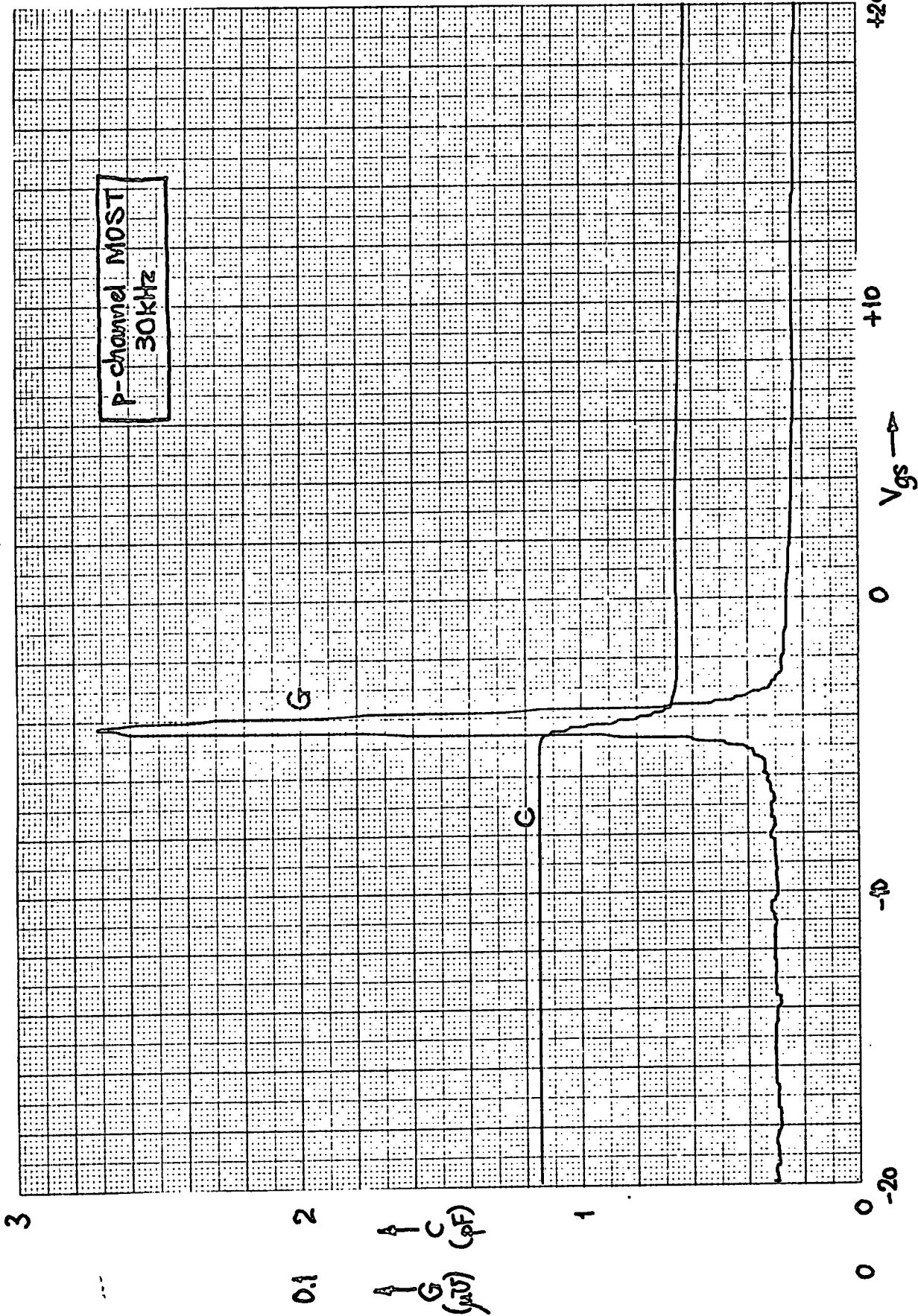states at the oxide-semiconductor interface.

Fig. 5-17: Actual X-Y recording of the C-V and G-V characteristics of a p-channel MOST.

– Chapter 6 –

THE I-V PLOTTER

6-1 Introduction

There is a need for an instrument capable of examining devices,

and contacts to devices, for ohmic or rectifying properties.

Until recently a Tektronix 575 Transistor Curve Tracer has been

used for this work in the Department, but this instrument has

two serious disadvantages:

(a) the swept voltage applied to devices is unipolar, so

   precluding examination of trace linearity at the origin; and

(b) when displaying low currents (10μA or less) the trace has

   loops due to phase shifts in the circuitry.

An instrument has been designed and built which overcomes

these problems, and which is used in conjunction with a standard

laboratory oscilloscope. The instrument accepts the sawtooth

timebase output of the oscilloscope, generates a variable

bipolar sweep voltage, and produces an output signal proportional

to the instantaneous device current.

6-2 Specification

The unit was designed to accept an oscilloscope output sweeping

Plate 6-1:   The I-V Plotter.

between +5 and +30V (Solartron CD1400 Series) or OV and
+25V (Cossor CDU110), and provide a swept voltage output
variable from zero to $\pm 150V$. The sensitivity of the current
detector was required to be switchable from luA cm^{-1} to
5mA cm^{-1}, assuming an oscilloscope Y-amplifier sensitivity of
100mV cm^{-1}.

To protect devices from over-dissipation, circuits were
included to limit device current to a value corresponding to
an oscill oscope deflection of $\pm 6cm$, regardless of the setting
of the current range switch.

The I-V Plotter was to have a self-contained mains power
supply.

6-3 Circuit details

The sweep generator circuit is designed to meet the specification
outlined in Section 6-2. It is based on a high-voltage power
amplifier (Q8 in Fig. 6-1) driven by an unconventional long-
tailed pair circuit, with overall negative feedback (R1, R2)
to determine the gain (40dB).

A high-voltage p-n-p transistor with a V_{ceo} rating of over
180V is synthesised by Q3-6. The 390kΩ base resistors ensure
uniform voltage sharing, but the input offset voltage created
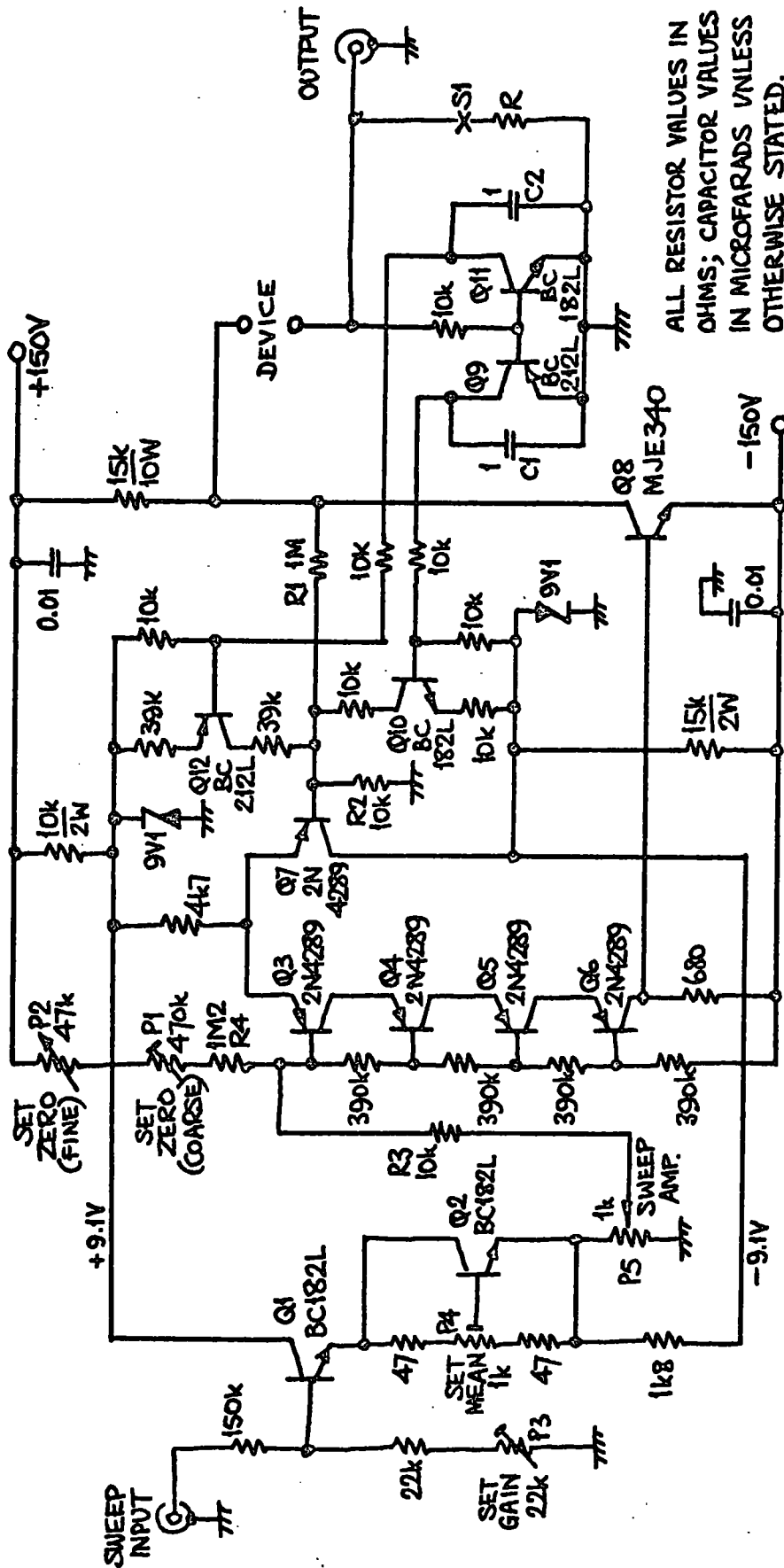across the 10kΩ resistor R3 must be cancelled by an opposing

Fig. 6-1: Circuit diagram of the I-V Plotter.

current through R4, P1 and P2. P2 is accessible at the rear of the instrument for setting zero output voltage (with the SWEEP AMPLITUDE control fully anticlockwise).

The incoming sawtooth waveform is attenuated to a level, set by P3, suitable for the main amplifier. Q1 is an emitter follower used to raise the input impedance of the instrument to about 170kΩ, and Q2 provides a d-c signal shift so that the output sweep voltage waveform is symmetrical about zero. The SET MEAN potentiometer P4 provides fine adjustment of symmetry. Sweep amplitude is controlled by the front-panel potentiometer P5.

Zener diode regulated supplies of both polarities are included in the circuit to reduce the number of high voltage transistors needed in the circuit.

The device current is measured from the voltage dropped across the current sensing resistor R. In normal use, the oscilloscope Y-amplifier (with 100mV sensitivity) is connected to this point. Current sensitivity is changed by switching R between 22Ω and 100kΩ, giving a range of 1uA cm^{-1} to 5 mA cm^{-1} in 1-2-5-10 sequence. The current-limiting circuits operate if the sensing voltage exceeds about 600mV. Q9 or Q11 conducts and, with Q10 or Q12, prevents any further increase in applied bias, by clamping the base of Q7. Negative current limiting is provided by Q9 and Q10; positive limiting by Q11 and Q12.

Because of the large number of active devices in the negative feedback loops associated with the current-limiting feature, high frequency instability was a serious problem. The circuit was stabilised by a dominant lag created by C1 and C2, each 1µF.

Fig. 6-2 shows the I-V Plotter power supply, which provides +150 and -150V stabilised. Some simplification was possible during design, as the current in the zero-volt rail is only 3mA. A high voltage transistor (Q1: Motorola MJE340) is used as a series stabiliser, using a reference voltage derived from two 150V regulator valves (V1, V2). The zero-volt rail is taken from the junction of the two.

6-4 Results and performance.

The I-V Plotter functions as expected, and successfully overcomes the disadvantages attributed to the Tektronix Transistor Curve Tracer. Precise measurements can be made down to about 200nA of device current. The Plotter has been used to measure the parameters of electroluminescent zinc selenide devices made in the Department, and will prove useful in the development of willemite-on-silicon devices. It is also planned to match microwave mixer diodes according to their slope resistance at the origin, using this instrument, for other work in the
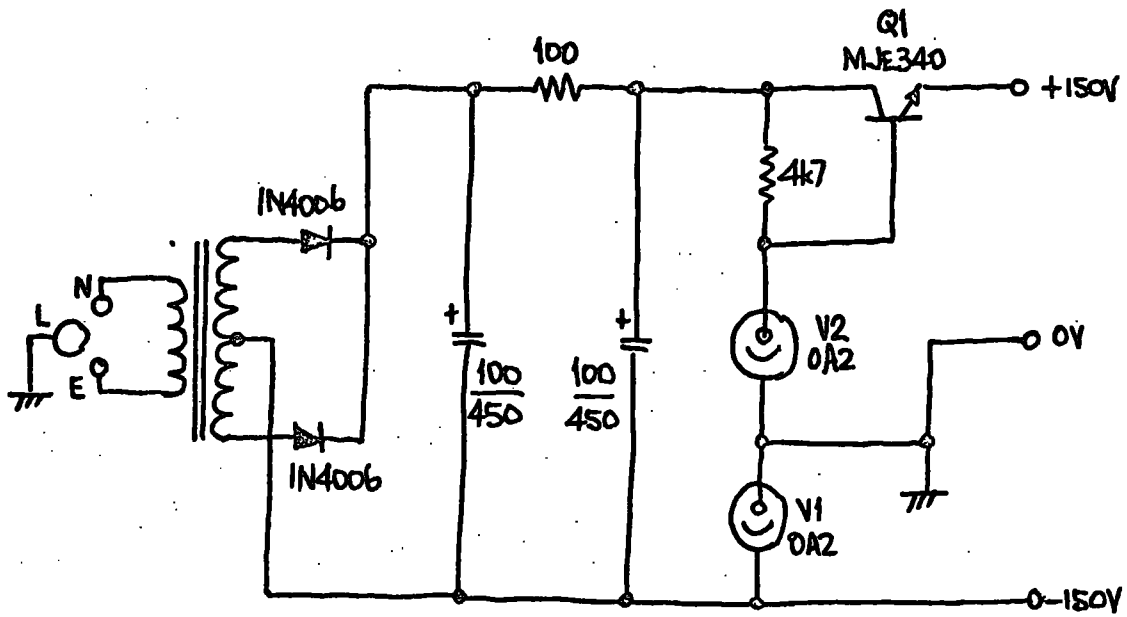
Fig. 6-2: Circuit diagram of the I-V Plotter power supply.

Department.

Any extension of the basic instrument sensitivity of
1 μA cm^{-1} by the use of higher oscilloscope sensitivity is
hindered by residual power supply ripple superimposed on the
sweep voltage waveform reaching the oscilloscope via the
device capacitance. More elaborate stabilisation of the
two supplies would improve this situation.

Fig. 6-3 is taken from an oscillograph of the I-V
characteristics of a point-contact germanium diode under low
current conditions. The behaviour of the diode at the origin
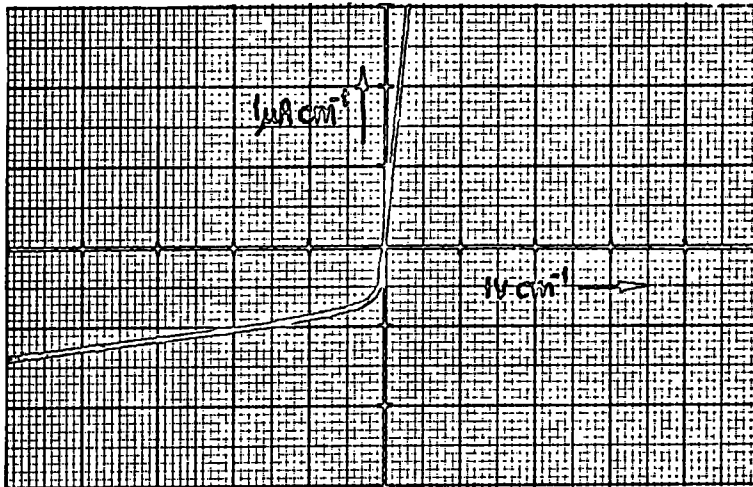is clearly seen.

Fig. 6-3: Copy of an oscillograph of the I-V characteristics of a Mullard OA81 germanium point-contact diode.

– Chapter 7 –

DISCUSSION

7-1 Assessment of the equipment

All the equipment described in this thesis functions

correctly under the operating conditions for which it was

intended, except that the electron beam evaporator has not yet

been used for the deposition of zinc fluoride onto silica.

In particular, the care taken in designing the G-C-V Plotter

has produced an extremely versatile instrument.

The electronic systems associated with the ultra-high

vacuum system (the ion pump power supply, bake-out heater

and bake-out controller) have operated unattended for periods

of over 50 hours without any faults developing.

The first C-V Plotter (Chapter 4) was used extensively

by Edwards [1] in the examination of his metal-willemite-

silicon (MWS) and metal-willemite-oxide-silicon (MWOS) devices,

and a model for the conduction processes was developed from the

results.

The G-C-V Plotter (Chapter 5) is capable of more accurate

work over a wide range of device admittances. In addition to high-frequency C-V curves, this Plotter provides low-frequency data and conductance-voltage curves. The performance of the G-C-V Plotter is considerably better than the instrument described by Shewchun and Waxman [6] in 1966. In particular the dynamic range has been improved by 40dB, and conductance and capacitance curves can be plotted simultaneously. The range of usable admittances and test frequencies has been extended.

Although the I-V Plotter has not yet been used in connection with willemite display devices, it has found several other applications in the Department where conventional transistor curve tracers have been unsuitable. This Plotter will be used to examine the second generation of display devices.

7-2 Conclusions

There are some   immediate suggestions for future work on equipment. An electron bombardment substrate heater must be built for the uhv system, and the second generation of willemite devices should be fabricated in the ultra-high vacuum environment. There is no doubt that the three plotting instruments will be invaluable when assessing the improvements brought about by these new techniques.

It has been suggested that light output measurements,

combined with further I-V experiments, are an early

requirement on any detailed study of the model postulated

for the physical behaviour of the thin films. In view of the

low device brightness achieved so far, this will involve some

advanced work with high-sensitivity photomultipliers or p-i-n

photodiodes, and wideband pulse amplifiers.

APPENDIX A

THE DOUBLE-BALANCED PHASE DETECTOR

The double-balanced phase-detector was developed by Danby [8] for a new range of instruments for detecting ultra-low level signals. The circuit is sufficiently interesting to warrant a description of its manner of operation and its performance. The circuit (originally Fig. 5-5) is reproduced overleaf.

The heart of the psd is the three interconnected long-tailed pair circuits with constant-current tail transistors (Q3, Q4 with Q2; Q6, Q7 with Q5; and Q2, Q5 with Q1). This configuration has similar properties to a four-diode ring modulator: it behaves as a mixer, and the output is balanced with respect to both inputs. It therefore functions as a psd whose single-ended output is independent of the mark-space ratio of the reference square-waves.

The circuit would function if the remaining transistors (Q8-11) were omitted, but the quiescent collector currents of Q4 and Q6 ($0 \cdot 5I_1$) would cause a d-c offset across R10 to appear at the output. The remainder of the circuit establishes the collector current of Q11 as exactly $0.5I_1$, so that the net quiescent current through R10 is zero.

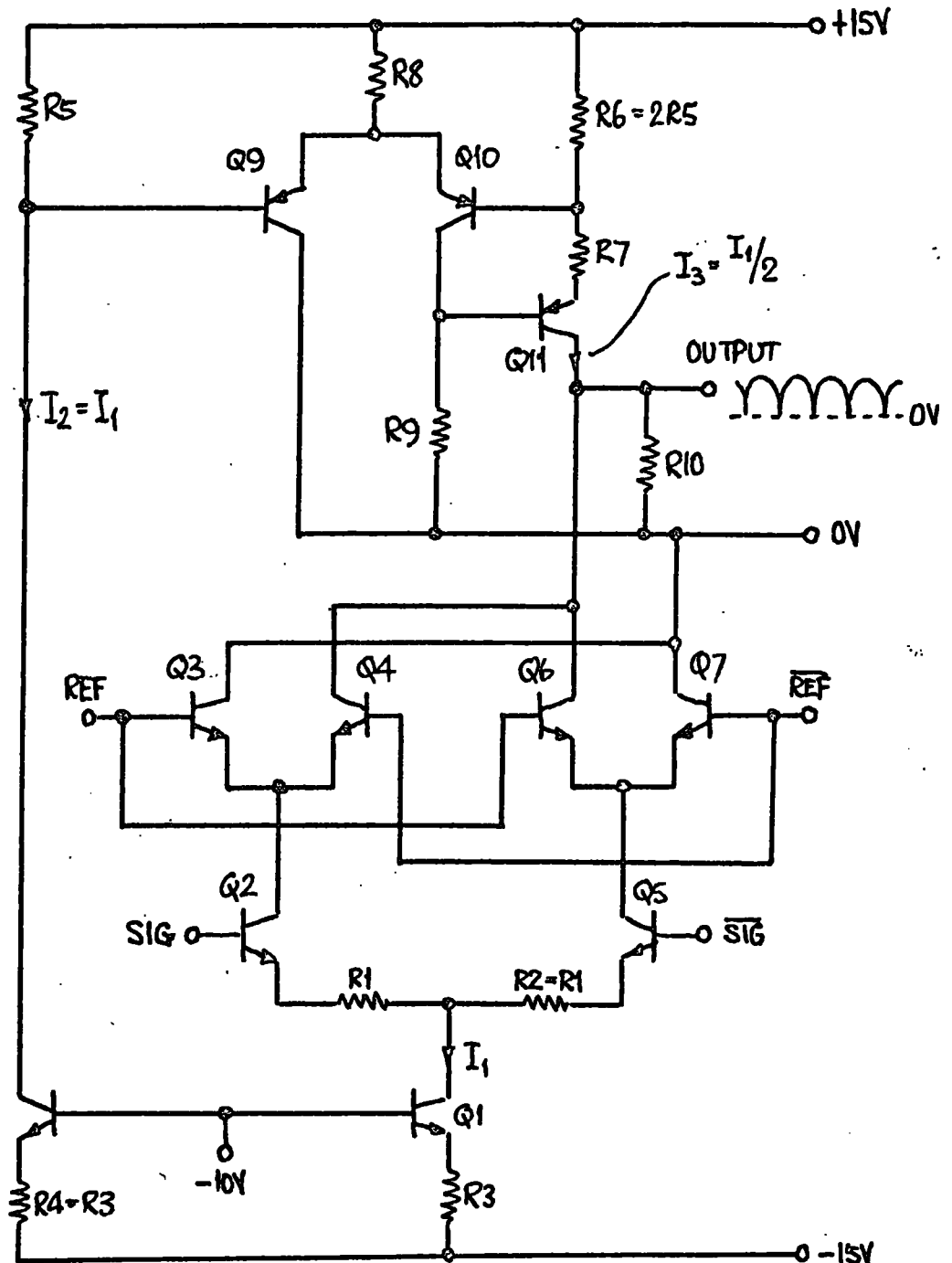R1 is equal to R2, so the quiescent current in the two

Fig. A-1: The double-balanced phase detector with output
offset compensation. (After Danby [8]).

switches is equal. Regardless of whether Q4 or Q6 is ON, with no input signal the output current is $0 \cdot 5I_1$. This must be supplied by the compensating circuit. As R4 equals R3, $I_2 = I_1$, regardless of temperature or changes in the +15V supply. Q9-11 form a negative feedback circuit to ensure that the base of Q10 follows the base of Q9, so that the ratio of $I_{C8}:I_{C10}$ is R6:R5. This is made 2:1 so that $I_3 = 0 \cdot 5I_1$ as required.

As would be expected in a double-balanced circuit of this type, intermodulation distortion is very low (less than 0.005%). The effect of out-of-phase signals is quoted as less than 0.01%, which is marginally better than the figure obtained for the G-C-V Plotter (0.02%). Danby claims that signals 70dB below the noise can be resolved with this circuit.

Transistors Q1 and Q8, Q9 and Q10, Q3 and Q4, and Q6 and Q7 are dual devices, to preserve the excellent temperature stability of the psd output.

99.

REFERENCES

[1]   "The Preparation and Properties of Luminescent Films on Silcon", G. S. Edwards, Ph.D. Thesis, Durham (1970), unpublished.

[2]   "Frequency Independent Directional Wattmeters and an SWR Meter", P. G. Martin, Radio Communication, 45, 399 (1969).

[3]   "The Use of Electron Beams in the Preparation of Epitaxial Silicon Films", J. Wales, Microelectronics and Reliability, 4, 91 (1965).

[4]   "Methods of Experimental Physics. Vol. 6A: Solid State Physics", p. 124.

[5]   "Investigation of Thermally Oxidised Silicon Surfaces using MOS Structures", A. S. Grove et al, Solid State Electron., 8, 145 (1965).

[6]   J. Shewchun and A. Waxman, Rev. Sci. Instr., 37, 1195 (1966).

[7]   "Ion Transport Phenomena in Insulating Films", E. H. Snow et al, J. Appl. Phys., 36, 1664 (1965).

[8]   "Circuit Configurations for Current-switching Phase-sensitive Detectors", P. C. G. Danby, Electronic Engineering, December 1968, p. 668.